Geometry Effects on the Electromagnetic Properties of Linear Magnetic Materials and Superconductors in the Critical State

Thesis project from

Enric Pardo Vivé

Bellaterra, January 2004

Acknowledgements

First of all, I acknowledge Dr. Àlvar Sánchez and Dr. Du-Xing Chen for the supervising of the thesis, without whom it could not be written. I do not only thank them the effort they put in it and their important contribution to the research but also the proximity and commitment they showed at any moment for the time during the supervising. However, for what I acknowledge them the most is for having been an example of scientific rigor and good research. I also acknowledge Dr. Carles Navau for his participation to my formation as a researcher in the early years of the doctorate, as well as for his contributions to the research.

I feel fortunate of having joined to our research group (Grup d'electromagnetisme, Departament de Física, Universitat Autònoma de Barcelona) for the friendly working atmosphere I have found, which members that I had more relation are, in alphabetical order, Dr. Àlvar Sánchez, Dr. Carles Navau, Dr. Du-Xing Chen, Dr. Fernando López Aguilar, Dr. Joan Costa Quintana, and the new students Nuria Del Valle and María Eckholt. I am grateful to Jordi Teva, thanks to whom I joined in Grup d'Electromagnetisme.

I acknowledge all the collaborators of the articles which I am coauthor, specially to F. Gömöry and coworkers from the Institute of Electrical Engineering in the Slovak Accademy of Sciences and A. Palau, T. Puig and X. Obradors from Institut de Ciència de Materials de Barcelona in Consejo Superior de Investigaciones Científicas. I would like to give extra acknowledgements to Dr. Fedor Gömöry for valuable discussions, thanks to whom we introduced to the topic of superconducting tapes. Apart from F. Gömöry, discussions with R. B. Goldfarb, S. Farinon, A. Badía, C. López, T. Puig, X. Obradors, A. Palau, X. Granados, and S. Takács are acknowledged.

To Fedor Gömöry I also thank the hospitality I recieved during my stay in the Institute of Electrical Engineering in Bratislava. For this reason I also acknowledge Frantisek, Eugen, Silvester Tákacs and all the staff in the Institute. Out of the Institute, I am grateful to Yuri, Ashraf, Maria, Dan and Raquel to make my stay in Bratislava a good experience. I also thank all those people with whom I went and met in conferences, making the experience easier.

With this thesis I finish an important stage of my live. In this sense and looking back, I do not want to miss the opportunity to thank many other people, just to be as they are. First, to Laia who represented another stage. And also, of course, all the old friends from Sabadell and from university, all the people I met in Edinburgh, Paris, Treforest (Cardiff) and Wien, and, why not, the members of the "Club de la Carmanyola".

I would also like to acknowledge my parents for having provided me a whole education and having given to me the necessary stability and sympathy to study a doctorate. For sure, this thesis would not be written without their implicit support. I also thank my brothers and sister; Rosa Anna and Tomàs for having awaken my interest to science and Carles for avoiding me to get obsessed with it.

I feel fortunate not to have to thank anybody for helping me in the hard times related to the thesis, since in the doctorate and the thesis itself there did not appear any hard period worth to mention.

Finally, I acknowledge "Departament d'Universitats, Recerca i Societat de la Informació" from "Generalitat de Catalunya" for the research fellowship grant 2000FI 00482.

Enric Pardo Vivé, Bellaterra 28 of January 2004.

Contents

CHAPTER 1

Introduction

The electromagnetic behavior of a certain material does not only depend on its intrinsic material properties but also on the shape of the sample being studied. Actually, some magnetic quantities in samples with the same material properties but different geometry can differ by several orders of magnitude. In this thesis we study the geometry effects, also called demagnetizing effects, in electromagnetic properties of both linear homogenous isotropic (LHI) materials and hard superconductors. For LHI materials we consider the response to a uniform applied field, while for hard superconductors we study both the cases of an applied ac magnetic field and a transport alternating current.

For magnetic samples immersed in a uniform applied field $\mathbf{H}_\mathrm{a}$, the magnetic field $\mathbf{H}$ inside the material is different from $\mathbf{H}_\mathrm{a}$ for realistic sample geometries due to demagnetizing effects. The magnetic field inside a magnetic material cannot be directly measured, but it may be determined theoretically. Moreover, $\mathbf{H}$ inside a sample is nonuniform for most practical geometries. One way to study $\mathbf{H}$ inside the material is by means of the fluxmetric and magnetometric demagnetizing factors N_f and N_m, respectively, which are directly related to the average $\mathbf{H}$ over the sample midplane and volume, respectively. The calculation of N_f and N_m can be therefore used to analyze most of the magnetic quantities of LHI materials, which makes $N_\mathrm{f,m}$ very useful for the experimental study of these materials. For example, they can be used to obtain the internal susceptibility χ from measurements of the magnetic flux in the midplane or the magnetic moment.

Although the first studies on demagnetizing factors were contemporary with Maxwell himself [1], the results had been very incomplete until the 1980s even for the regular geometries of rectangular prisms and cylinders. The lack of theoretical studies is due to the difficulty in obtaining analytical results of $N_\mathrm{f,m}$, so that for most cases numerical calculations are needed. The development of personal computers made possible accurate numerical calculations for some cases [2, 3, 4, 5, 6]. The aim of this thesis concerning

demagnetizing factors is to calculate their values for rectangular prisms for a wide range of susceptibility and aspect ratios, a geometry with very few existing theoretical results. When possible we deduce $N_{\mathrm{f,m}}$ analytically, otherwise we perform accurate numerical calculations using an ordinary personal computer.

Apart from LHI materials we study hard superconductors, which are materials very interesting for applications. These materials are nonlinear and hysteretic, so that the use of the results for LHI materials is very limited. A possible way to describe the electromagnetic properties of hard superconductors is by means of the critical-state model [7, 8, 9], which assumes that the magnitude of the nonzero current density has a constant value. In spite of the simplicity of this model, the application to geometries with a finite dimension along the applied field requires a further development of the model and results have to be obtained by numerical calculations. These are the reasons for the existence of very few results, even for geometries with an infinitely long dimension, which mathematically can be reduced to two dimensions.

Concerning hard superconductors, we present a careful systematical study of electromagnetic properties for some infinitely long geometries under transverse applied ac magnetic field or a transport alternating current. This study is interesting for applications of superconducting tapes and wires in electrical devices operating in ac regime, being the ac loss one of the most relevant quantities.

This thesis is structured as follows. First, in chapter 2 we introduce the general theoretical framework of this thesis. We present and review the main quantities and properties concerning the demagnetizing effects and the demagnetizing factors, concentrating in LHI materials. We also summarize the characterizing magnetic and transport properties of superconductors, specifically those for hard superconductors. The original critical-state model, which is commonly used to describe hard superconductors, is presented and discussed as well. We note that SI units are used throughout the thesis.

In chapters 3, 4, and 5 we present our study on demagnetizing factors for LHI materials, while chapters 6, 7, and 8 deal with infinitely long hard superconductors. In chapter 3 we review the most important existing theoretical results on $N_{\mathrm{f,m}}$ for rectangular prisms and cylinders. We also present a numerical procedure in a general formulation to calculate the demagnetizing factors for LHI samples with arbitrary susceptibility, based on a previously existing model for cylinders [3]. We do not only generalize the procedure for cylinders to other geometries but also introduce an improvement which reduces computation time and increases accuracy.

In chapter 4, we calculate and discuss the demagnetizing factors for infinitely long rectangular prisms with transverse applied field for a wide range of values of susceptibility and width-to-thickness aspect ratio. For some special values of susceptibility, $N_{\mathrm{f,m}}$ is calculated analytically, while for the others we use the numerical procedure presented in chapter 3. The analytical results can be compared with the numerical results in order to estimate and reduce the error in the numerical calculations of $N_{\mathrm{f,m}}$. Moreover, we also present a way to calculate N_{m} for cylinders in the radial direction from existing results for N_{m} in the axial direction.

The demagnetizing factors for rectangular prisms are numerically calculated and discussed in chapter 5. There, we present the main features concerning the adaptation of the numerical method formulated in chapter 3 to the rectangular prism geometry, which has been possible thanks to the experience achieved for infinitely long rectangular prisms in chapter 4. The case of finite rectangular prisms involves an extra parameter (another aspect ratio) as compared to infinitely long ones, so that one needs to perform many more calculations to make a complete study of $N_{\mathrm{f,m}}$ for this geometry. For this reason, we first study the specific cases with practical importance of square bars, which only have one aspect ratio, and perfectly shielded rectangular prisms, for which the susceptibility is fixed. The experience achieved with these two systems is very useful to accurately calculate and analyze the general case of rectangular prisms with arbitrary susceptibility, which is being calculated by the time of writing this thesis.

After the study of demagnetizing effects in LHI materials, in chapters 6, 7 and 8 we present a systematic study of the magnetic properties of infinitely long hard superconductors with a transverse applied ac field or an alternating transport current.

This study is done by numerical calculations using a procedure based on magnetic energy minimization (MEM) considering the critical-state model with a constant critical-current density. This procedure is developed in chapter 6 for infinitely long geometries with constant cross-section, including multifilamentary structures. For the magnetic case with multifilamentary cross-sections we consider both the situation of mutually electrically isolated filaments, which have the restriction of net current to be zero inside each filament, and filaments interconnected at infinity, without such a restriction. We also discuss some results achieved using the MEM procedure to other situations, such as levitation systems or granular YBCO coated conductors.

We present in chapter 7 a systematic theoretical study of the magnetic properties, such as current density, magnetization loops, ac susceptibility, and ac loss for some infinitely long geometries under transverse applied ac magnetic field. The geometries studied are rectangular bars (strips), elliptical bars, and some regular arrangements of strips, such as linear arrays in the applied-field direction (vertical stacks) or perpendicular to it (horizontal arrays), matrix arrays, and interleaved configurations.

The situation of an alternating current being transported through infinitely long superconducting samples is studied in chapter 8. In this chapter we consider the geometries of a single strip, linear arrays of strips, and matrices, for which the current profiles and the ac loss are calculated.

Finally, in chapter 9 we present the conclusions of this thesis.

CHAPTER 2

General concepts

In this chapter the main concepts involved in the thesis are reviewed. First, we present the theoretical frame related to the demagnetizing effects and, subsequently, a summary on the main properties of superconductors, where the critical sate is formulated.

2.1 A summary of some magnetic quantities

This section provides the fundamentals of the demagnetizing effects, that is, the effects on the magnetic properties in a material due to sample geometry. Moreover, in this section we introduce the formulation that is used throughout the thesis.

2.1.1 Magnetic moment and magnetization

In classical magnetostatics the dipolar magnetic moment $\mathbf{m}$ created by a certain current density $\mathbf{J}$ is [10, 11, 12]

$$\mathbf{m} = \frac{1}{2}\int_V \mathbf{r} \times \mathbf{J}(\mathbf{r})\mathrm{d}V, \tag{2.1}$$

where V is the volume where the current is present. In a magnetic material, apart from the moment of macroscopic currents which can flow through the whole sample, there are other localized microscopic magnetic moments, which have a quantum-mechanical origin. When these microscopic moment sources have much smaller dimensions than the considered length scales, we can define the local magnetization $\mathbf{M}(\mathbf{r})$ as a local magnetic moment density $\mathbf{M} = \mathrm{d}\mathbf{m}/\mathrm{d}V$. This local magnetization must be distinguished from the volume average magnetization $\mathbf{M}_{\mathrm{vol}} \equiv \mathbf{m}/V$, which can be due to either a free current density J or microscopic magnetic moment sources.

2.1.2 Magnetic field and magnetic induction

We next review the differential equations and boundary conditions in magnetostatics, which are the basis of the calculations presented in this thesis. The fundamental equations in magnetostatics are [10, 11, 12]

$$\nabla \times \mathbf{H} = \mathbf{J}, \tag{2.2}$$

$$\nabla \cdot \mathbf{B} = 0, \tag{2.3}$$

where $\mathbf{H}$ is the magnetic field strength, $\mathbf{B}$ is the magnetic induction and $\mathbf{J}$ is the free current density. Equation (2.2) is named the Ampère law. The boundary conditions of Eqs. (2.2) and (2.3) on the interface between two magnetic media are

$$(\mathbf{H}_1 - \mathbf{H}_2) \times \mathbf{e}_\mathrm{n} = 0 \tag{2.4}$$

$$(\mathbf{B}_1 - \mathbf{B}_2) \cdot \mathbf{e}_\mathrm{n} = 0. \tag{2.5}$$

where subindices '1' and '2' refer to each magnetic medium and $\mathbf{e}_\mathrm{n}$ is the unit vector perpendicular to the interface pointing outwards medium 1.

The magnetic field and the magnetic induction are related to each other by means of the magnetization as

$$\mathbf{B} = \mu_0(\mathbf{H} + \mathbf{M}), \tag{2.6}$$

where μ_0 is the permeability of free space. Considering this, Eqs. (2.2) and (2.4) can also be written as a function of the magnetic induction as

$$\nabla \times \mathbf{B} = \mu_0 \left(\mathbf{J} + \mathbf{J}_M\right), \tag{2.7}$$

$$(\mathbf{B}_1 - \mathbf{B}_2) \times \mathbf{e}_\mathrm{n} = \mu_0 \mathbf{K}_M, \tag{2.8}$$

where $\mathbf{J}_M$ and $\mathbf{K}_M$ are the current density and sheet current density, respectively, and are defined as

$$\mathbf{J}_M \equiv \nabla \times \mathbf{M}, \tag{2.9}$$

$$\mathbf{K}_M \equiv (\mathbf{M}_1 - \mathbf{M}_2) \times \mathbf{e}_\mathrm{n}. \tag{2.10}$$

From Eqs. (2.8) and (2.10) we see that the discontinuities of the magnetic induction are due to discontinuities in magnetization.

Time-varying current density

In some discussions of this thesis we shall consider time-varying magnetic quantities. For all the studied situations, we assume the quasi-static approximation, that is, the displacement current is neglected, so that Eq. (2.2) is still valid [10, 11, 12]. Considering this, a time-varying J generates a time-varying $\mathbf{H}$ and $\mathbf{B}$ [Eqs. (2.2), (2.3) and (2.6)], which creates an electrical field $\mathbf{E}$ due to the Faraday law

$$\nabla \times \mathbf{E} = -\frac{\partial \mathbf{B}}{\partial t}. \tag{2.11}$$

As a consequence of this electrical field, there appears a power dissipation P as

$$P = \int \mathrm{d}V \, \mathbf{J} \cdot \mathbf{E}. \tag{2.12}$$

Pole density and magnetic scalar potential

In many actual situations, there is no free current in the magnetic materials, so that $\mathbf{J} = 0$. In this case, equations (2.2), (2.3), (2.4) and (2.5) can be written in terms of $\mathbf{H}$ by using Eq. (2.6) as

$$\begin{aligned} \nabla \times \mathbf{H} &= 0, & (2.13)\\ \nabla \cdot \mathbf{H} &= \rho_M, & (2.14)\\ (\mathbf{H}_1 - \mathbf{H}_2) \times \mathbf{e}_\mathrm{n} &= 0, & (2.15)\\ (\mathbf{H}_1 - \mathbf{H}_2) \cdot \mathbf{e}_\mathrm{n} &= -\sigma_M, & (2.16) \end{aligned}$$

where ρ_M and σ_M are the volume and surface pole densities defined as

$$\begin{aligned} \rho_M &\equiv -\nabla \cdot \mathbf{M}, & (2.17)\\ \sigma_M &\equiv (\mathbf{M}_1 - \mathbf{M}_2) \cdot \mathbf{e}_\mathrm{n}. & (2.18) \end{aligned}$$

From Eqs. (2.16) and (2.18) we see that the discontinuities in $\mathbf{H}$ are due to discontinuities in $\mathbf{M}$.

The differential equations and boundary conditions for the magnetic field $\mathbf{H}$ in magnetostatics, Eqs. (2.13)-(2.16), have the same form as these for the electric field $\mathbf{E}$ in electrostatics with charge densities ρ_E and σ_E. The electrostatics equations are obtained after replacing $\mathbf{H}$ by $\mathbf{E}$, ρ_M by ρ_E and σ_M by σ_E. Thanks to this analogy, all the solutions obtained for electrostatics are also valid for magnetostatics without free currents.

Moreover, same as for the electric field, the magnetic field lines start in positive magnetic poles, end in negative ones and never form closed loops. These issues can be directly deduced from Eqs. (2.13) and (2.14).

Thanks to $\nabla \times \mathbf{H} = 0$, we can describe the magnetic field by means of a magnetic scalar potential ϕ so that $\mathbf{H} = -\nabla\phi$. This completes the analogy with the electrical field, since $\mathbf{E} = -\nabla\phi_E$ owing to $\nabla \times \mathbf{E} = 0$.

2.1.3 Magnetic susceptibility. Linear homogenous isotropic materials

The magnetic susceptibility χ is defined by the relation

$$\mathbf{M}(\mathbf{r}) = \chi(\mathbf{H}, \mathbf{r})\mathbf{H}(\mathbf{r}). \tag{2.19}$$

Since the magnetization and the magnetic field are not necessarily parallel, the magnetic susceptibility is in general a tensor. Moreover, χ can depend on the position and the magnetic field.

A linear homogeneous isotropic (LHI) material is defined as a material for which χ is a scalar number (isotropic) independent of the magnetic field (linear) and position (homogeneous), so that the local relation $\mathbf{M}(\mathbf{r}) = \chi\mathbf{H}(\mathbf{r})$ holds, where χ is a real number. As a consequence, the magnetic response of a material is determined by a single parameter. A LHI material can also be characterized by the magnetic permeability μ, defined as $\mu = \mu_0(1 + \chi)$. Then, from the $\mathbf{H}$ and χ definitions we obtain

$$\mathbf{B} = \mu\mathbf{H}. \tag{2.20}$$

The magnetic susceptibility χ must be distinguished from the external susceptibility χ^{ext}, which is defined from

$$\mathbf{M}_{\text{vol}} = \chi^{\text{ext}}\mathbf{H}_{\text{a}}, \tag{2.21}$$

$\mathbf{M}_{\text{vol}}$ being the magnetization averaged over the sample volume and $\mathbf{H}_{\text{a}}$, the uniform external applied field. We note that the χ^{ext} relates nonlocal quantities, different from χ in Eq. (2.19).

Moreover, for LHI materials presenting no free-current density the magnetization follows

$$\nabla \times \mathbf{M} = 0, \tag{2.22}$$

$$\nabla \cdot \mathbf{M} = 0, \tag{2.23}$$

which can be deduced from Eqs. (2.3), (2.6) and (2.13). Equations (2.22) and (2.23) imply that in the sample volume $\mathbf{J}_M = 0$ and $\rho_M = 0$, respectively. However the magnetization current and the pole density can be nonzero on the sample surface.

The magnetic susceptibility can, in principle, take any value between -1 and ∞. $\chi = -1$, ∞ and 0 are specific cases of importance.

The $\chi \to \infty$ limit is commonly used to describe ferromagnetic materials under certain conditions. Ferromagnetic materials are hysteretic, although the magnetization loop, obtained after increasing and decreasing H_{a}, is almost linear far away from saturation, presenting a high slope. The slope of the initial magnetization curve for low H_{a} can range from few hundreds for iron up to 10^5 for permalloy. The approximation of $\chi = \infty$ for materials with high susceptibility is valid for not very long samples in the direction of the applied field (Sec. 4.2.3) [3, 13]. In addition, from Eq. (2.20) we can deduce that for infinite susceptibility the magnetic field $\mathbf{H}$ is zero inside the sample.

Besides weak magnetic materials, $|\chi| \ll 1$, the case $\chi = 0$ also describes saturated ferromagnetic materials. This is so because ferromagnetic materials present uniform and field-independent magnetization under enough high applied fields.

Finally, the $\chi = -1$ ($\mu = 0$) case corresponds to the perfect magnetic shielding situation, since $\mathbf{B} = 0$ inside the material for any $\mathbf{H}$, Eq. (2.20). An example of this case is a superconductors in Meissner state with London penetration depth much lower than the sample dimensions (Sec. 2.3.1).

Differential equations for the electromagnetic potential

In LHI materials with no free currents, both the magnetic induction and magnetic field can be found by means of two different sets of differential equations, Eqs. (2.7), (2.3), (2.8), (2.5) or Eqs. (2.13)-(2.16), thanks to the relation $\mathbf{B} = \mu\mathbf{H}$.

Equations (2.7), (2.3), (2.8) and (2.5) can be written as function of the vector potential $\mathbf{A}$ by using $\mathbf{B} = \nabla \times \mathbf{A}$. The field equation considering the gauge $\nabla \cdot \mathbf{A} = 0$ reduces to

$$\nabla^2 \mathbf{A} = 0. \tag{2.24}$$

The boundary conditions for a sample with permeability μ_1 immersed in a magnetic material with permeability μ_2 are in the materials interface

$$\mathbf{e}_\mathrm{n} \times (\mathbf{A}_1 - \mathbf{A}_2) = 0, \tag{2.25}$$

$$\mathbf{e}_\mathrm{n} \times \left(\frac{1}{\mu_1} \nabla \times \mathbf{A}_1 - \frac{1}{\mu_2} \nabla \times \mathbf{A}_2 \right) = 0, \tag{2.26}$$

which can be deduced from Eqs. (2.5) and (2.15).

If the magnetic scalar potential ϕ is preferred to describe the magnetic system, one obtains the field equation

$$\nabla^2 \phi = 0, \tag{2.27}$$

deduced from Eqs. (2.13) and (2.14) using $\mathbf{H} = -\nabla\phi$. Again, the boundary conditions in the interface can be deduced from Eqs. (2.5) and (2.15), yielding to

$$\mathbf{e}_\mathrm{n} \cdot (\mu_1 \nabla\phi_1 - \mu_2 \nabla\phi_2) = 0, \tag{2.28}$$

$$\phi_1 = \phi_2. \tag{2.29}$$

In many practical cases, the magnetic sample is immersed in a uniform applied field $\mathbf{H}_\mathrm{a}$. In this case, boundary conditions at infinity must be considered, which are

$$\nabla \times \mathbf{A} = \mu_2 \mathbf{H}_\mathrm{a}, \tag{2.30}$$

$$\nabla\phi = -\mathbf{H}_\mathrm{a} \tag{2.31}$$

for the vector potential and the scalar potential, respectively.

2.2 Demagnetizing effects

The magnetic behavior of a sample does not only depend on its intrinsic magnetic properties, such as $\mathbf{M}$ or χ for LHI materials, but also on its geometry, as can be seen from the boundary conditions for $\mathbf{H}$ and $\mathbf{B}$ in Sec. 2.1.2. The effects of the geometry of the sample on their magnetic properties are usually known as demagnetizing effects.

The demagnetizing effects can change $\mathbf{B}$, $\mathbf{H}$ or $\mathbf{M}$ by some orders of magnitude when comparing between samples with the same intrinsic magnetic properties but with different geometry (see chapters 4 and 5). Then, a deep understanding of the demagnetizing effects is of vital importance to extract the intrinsic magnetic properties of a sample from magnetic measurements.

2.2.1 Demagnetizing fields

As presented in Sec. 2.1, a magnetic field **H** can be generated by either free currents or some pole distribution due to the sample magnetization [14] by means of Eqs. (2.2)-(2.16). The magnetic field generated by the pole density is called the demagnetizing field, $\mathbf{H}_\mathrm{d}$. In many magnetic measurements there are no free currents in the sample, so that Eqs. (2.13)-(2.16) can be used and the analogy to electrostatics is fulfilled.

In LHI materials (Sec. 2.1.3), the pole density in the sample volume is zero, although these materials can present nonzero surface pole density.

If $\chi > 0$ and the volume average magnetization $\mathbf{M}_\mathrm{vol}$ is parallel to the applied field[1], there appears a surface pole density like in Fig. 2.1(a,b). As for the electrical field, the magnetic field lines are created in the positive pole density zones and annihilated where negative pole density is present. As shown in Fig. 2.1(a,b), $\mathbf{H}_\mathrm{d}$ in the sample interior has roughly the sense opposite to that of the applied field, so that the magnitude of the total magnetic field in the sample interior is lower than the applied field. Then, the magnitude of the magnetization in the sample is lower than $|\chi \mathbf{H}_\mathrm{a}|$, which is the value we would expect if there was no demagnetizing field. For the limit of $\chi \to \infty$ the total magnetic field inside the sample is zero [Eq. (2.20)], so that the demagnetizing field inside the sample is uniform and opposite to the applied field, Fig 2.1(a).

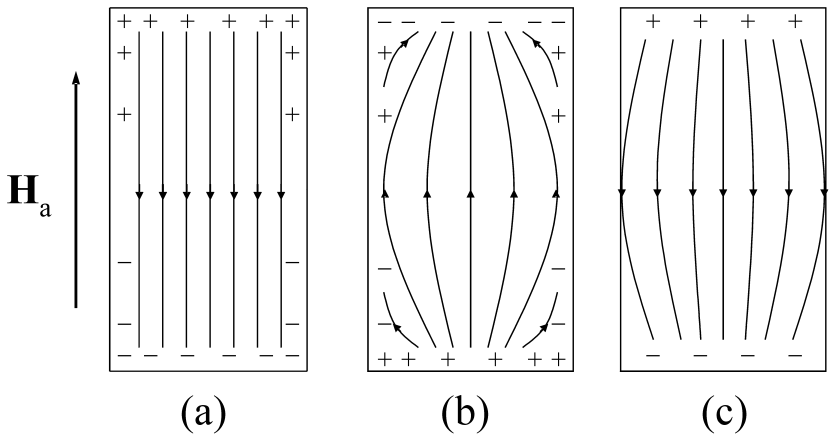

Figure 2.1: Sketch of the demagnetizing field $\mathbf{H}_\mathrm{d}$ created by the pole density σ_M in a sample submitted to a uniform applied field $\mathbf{H}_\mathrm{a}$. The sketch is qualitatively correct for a vertical cut of a cylinder or a rectangular bar. The figures correspond to $\chi = \infty$ (a), $0 > \chi \geq -1$ (b) and $\chi \to 0^+$ with uniform magnetization (c).

For $\chi < 0$, the magnetization has opposite direction to the applied field. As a consequence, the pole density at the sample ends has the opposite sign to that for $\chi > 0$, Fig. 2.1. Then, the demagnetizing field has the same direction as the applied

[1] If the sample geometry has some mirror symmetry, $\mathbf{M}_\mathrm{vol}$ is parallel to $\mathbf{H}_\mathrm{a}$ for $\mathbf{H}_\mathrm{a}$ perpendicular to the plane symmetry.

field and $H > H_\mathrm{a}$, so that the magnetization is higher than if only the external field was present. Moreover, the pole density on the side surfaces has opposite signs than on the end ones [3].

For uniform magnetization or the limit $\chi \to 0$, the surface pole density becomes uniform on the end surface and zero on the side ones. However, the demagnetizing field is not uniform [Fig. 2.1(c)]. This apparent contradiction is solved as follows. Although $\mathbf{H}_\mathrm{d}$ is not uniform, for $\chi \to 0$ the magnetization is much lower than the applied field, so that the pole density is very small and creates a low demagnetizing field. Then, $H_\mathrm{d} \ll H_\mathrm{a}$ and the magnetic field inside the sample is almost the applied field, which is uniform. As a consequence, the magnetization can be taken as uniform and parallel to the applied field. For saturated spin systems, the apparent contradiction is resolved in the same way as for $\chi \to 0$ provided that the applied field is high enough, so that $H_\mathrm{a} \gg M$ [15].

The effect of $\mathbf{H}_\mathrm{d}$ on the magnetization for $\chi > 0$ is the reason why the demagnetizing field is called in this way, although for negative susceptibility $\mathbf{H}_\mathrm{d}$ enhances the magnitude of the magnetization.

Since $\mathbf{H}_\mathrm{d}$ is created by the surface pole density, which is due to the magnetization component normal to the sample surface, the demagnetizing field strongly depends on the sample geometry. As it is explained below, the demagnetizing field can change the magnetization by some orders of magnitude.

The demagnetizing field has effects not only on the magnetization but also on the external magnetic field and the total magnetic field at any point (inside or outside the body) is

$$\mathbf{H} = \mathbf{H}_\mathrm{a} + \mathbf{H}_\mathrm{d}, \tag{2.32}$$

where $\mathbf{H}_\mathrm{a}$ is the applied field, which is created by some external electrical current or magnetic pole density and it is usually assumed to be independent of the sample magnetization.

Magnetization induction and demagnetizing field

An alternative way to describe the demagnetizing effects is to use the magnetic induction $\mathbf{B}$, that is generated by both free currents and magnetization currents Eqs. (2.3), (2.7), (2.5) and (2.8). In the absence of free currents, the only magnetic induction sources are magnetization currents. The magnetic induction created by these magnetization currents is called the magnetization induction $\mathbf{B}_M$. If the sample is immersed in an external magnetic field the total magnetic induction is

$$\mathbf{B} = \mu_0 \mathbf{H}_\mathrm{a} + \mathbf{B}_M. \tag{2.33}$$

For LHI materials, there are no volume magnetization currents (Sec. 2.1.3), so that $\mathbf{B}_M$ is created by the surface magnetization currents $\mathbf{K}_M$ only.

The concepts of magnetization induction $\mathbf{B}_M$ and demagnetizing field $\mathbf{H}_\mathrm{d}$ are similar in the sense that they are the contributions to $\mathbf{B}$ and $\mathbf{H}$, respectively, due to the mag-

netization of the sample. Moreover, for LHI materials we can find a relation between $\mathbf{B}_M$ and $\mathbf{H}_\mathrm{d}$ by means of Eqs. (2.20), (2.32) and (2.33). This relation is

$$\mathbf{B}_M = \mu_0(1+\chi)\mathbf{H}_\mathrm{d} + \mu_0\chi\mathbf{H}_\mathrm{a}. \tag{2.34}$$

Equation (2.34) is useful to obtain the demagnetizing field when only the magnetization currents, from which $\mathbf{B}_M$ can be deduced, are known.

2.2.2 Demagnetizing factors

There are many magnetic measurements performed under a uniform external applied field $\mathbf{H}_\mathrm{a}$ over the sample. In chapters 3, 4 and 5 we will focus on two commonly performed magnetic measurements. These are the fluxmetric (or ballistic) measurements and the magnetometric measurements.

In fluxmetric measurements, the magnetic flux Φ is measured over a cross-section of the sample, typically the midplane. The corresponding average magnetic induction B_mid can be obtained dividing by the cross-section surface. A possible way to measure Φ can be done by winding a thin coil around the cross-section of the sample, applying a uniform applied ac field and then measuring the electromotive force in the coil.

The quantity directly obtained in magnetometric measurements is the magnetic moment m, from which M_vol can be obtained dividing by the sample volume. There exist many different techniques based on several physical mechanisms to do magnetometric measurements. Some of them are based on measurements of magnetic flux in some space region under uniform applied fields [16, 17]. Other techniques extract the magnetic moment from the magnetic force on the sample in the presence of a nonuniform external field.

Measurements of Φ or m are often not enough to extract the intrinsic magnetic properties of the samples. For example, in order to obtain χ for a LHI material from Φ or m, the determination of $\mathbf{H}$ is also necessary, or at least its average on the cross-section or the volume (H_mid and H_vol, respectively). Although the applied magnetic field in the sample is usually known, the demagnetizing field strongly depends on the sample geometry, which is not easy to calculate or to determine experimentally.

In order to consider the effect of demagnetizing fields in fluxmetric and magnetometric measurements, it is useful to define the fluxmetric and magnetometric demagnetizing tensors $\mathbf{N}_\mathrm{f}$ and $\mathbf{N}_\mathrm{m}$ as

$$\mathbf{H}_\mathrm{d,mid,vol} = -\mathbf{N}_\mathrm{f,m}\mathbf{M}_\mathrm{mid,vol}, \tag{2.35}$$

where the subindices 'mid' and 'vol' refer to the average over the midplane and the volume, respectively. In general, $\mathbf{H}_\mathrm{d,mid,vol}$ and $\mathbf{M}_\mathrm{mid,vol}$ do not have to be parallel to each other, even if the magnetic material is LHI, because the geometry of the sample do not have to be symmetric.

For the cases that $\mathbf{B}_\mathrm{mid,vol}$, $\mathbf{M}_\mathrm{d,mid,vol}$ and $\mathbf{H}_\mathrm{d,mid,vol}$ are parallel to the applied field $\mathbf{H}_\mathrm{a}$, we can ignore the vectorial nature of these quantities. Then, the demagnetizing

tensor is reduced to a number, which receives the name of demagnetizing factor and can be defined as [3]

$$N_{\mathrm{f,m}} = -H_{\mathrm{d,mid,vol}}/M_{\mathrm{mid,vol}}. \tag{2.36}$$

The directions of $\mathbf{H}_{\mathrm{a}}$ for which all the averaged magnetic quantities are parallel to and the demagnetizing tensor is reduced to a scalar are called as principal directions. For LHI materials the directions perpendicular to a plane of mirror symmetry are always principal directions. This is because for this case the magnetic pole distribution is antisymmetric with respect to the mirror symmetry plane (Fig. 2.1) so that $\mathbf{H}_{\mathrm{d,mid,vol}}$ is perpendicular to the symmetry plane and, consequently, parallel to $\mathbf{H}_{\mathrm{a}}$. For LHI materials the average magnetization and average magnetic induction are also parallel to the applied field thanks to $\mathbf{M} = \chi(\mathbf{H}_{\mathrm{a}} + \mathbf{H}_{\mathrm{d}})$ and $\mathbf{B} = \mu(\mathbf{H}_{\mathrm{a}} + \mathbf{H}_{\mathrm{d}})$, respectively.

If the applied field is parallel to a principal direction, the magnetic moment and the external susceptibility, defined in Eq. (2.19), can be written as a function of N_{m} by means of Eqs. (2.32) and (2.36) as

$$\chi^{\mathrm{ext}} = \frac{m}{H_{\mathrm{a}}V} = \frac{1}{N_{\mathrm{m}} + 1/\chi}, \tag{2.37}$$

where V is the sample volume. If the χ dependence of N_{m} is known, this relation allows the extraction of χ from magnetometric measurements. We can obtain a similar relation concerning the magnetic flux Φ over the midplane and N_{f}, so that

$$\frac{\Phi}{\mu_0 H_{\mathrm{a}} S} = \frac{1 + 1/\chi}{N_{\mathrm{f}} + 1/\chi}, \tag{2.38}$$

being S the surface of the midplane. This is one of the reasons why we systematically calculate $N_{\mathrm{f,m}}$ for several χ in chapters 4 and 5.

To determine the demagnetizing factors $N_{\mathrm{f,m}}$ we need both $H_{\mathrm{d,mid,vol}}$ and $M_{\mathrm{mid,vol}}$. However, if the material is LHI, the magnetization is related to the magnetic field as $\mathbf{M} = \chi\mathbf{H}$ and, consequently, the demagnetizing factors can be written as a function of either $H_{\mathrm{d,mid,vol}}$ or $M_{\mathrm{mid,vol}}$. Using Eq. (2.32), we deduce from Eq. (2.36) that

$$N_{\mathrm{f,m}} = \frac{H_{\mathrm{a}}}{M_{\mathrm{mid,vol}}} - \frac{1}{\chi}, \tag{2.39}$$

$$N_{\mathrm{f,m}} = \frac{-H_{\mathrm{d,mid,vol}}}{\chi(H_{\mathrm{d,mid,vol}} + H_{\mathrm{a}})}. \tag{2.40}$$

We notice that Eq. (2.40) is not useful for $\chi = \infty$ and that neither Eqs. (2.39) nor (2.40) are useful for $\chi = 0$ because they lead to mathematical indeterminations. Furthermore, if only the magnetization induction B_M is known, the demagnetizing fields can be obtained using Eqs. (2.34) and (2.40) so that

$$N_{\mathrm{f,m}} = \frac{\chi H_{\mathrm{a}} - B_{M,\mathrm{mid,vol}}/\mu_0}{\chi(B_{M,\mathrm{mid,vol}}/\mu_0 + H_{\mathrm{a}})}, \tag{2.41}$$

where $B_{M,\mathrm{mid,vol}}$ is the mean magnetization induction in the midplane and the volume, respectively. In a similar way than for Eqs. (2.39) and (2.40), Eq. (2.41) is not useful for $\chi = -1$ since for this case $\mathbf{B}_M = -\mu_0 \mathbf{H}_\mathrm{a}$ and Eq. (2.41) results in an indetermination.

It is also important to mention that for a uniform magnetization sample ($\chi = 0$), the magnetometric demagnetizing factors in the principal directions follow

$$N_{\mathrm{m},x} + N_{\mathrm{m},y} + N_{\mathrm{m},z} = 1, \tag{2.42}$$

according to [18, 15, 19, 20]. In Eq. (2.42) we took the directions of x, y and z as principal directions.

The demagnetizing factors for an infinitely long sample with constant cross-section are zero for an applied field in the long direction. This is so because the system made up of the sample and the infinite applied field has translational symmetry in the infinite direction, so that $\mathbf{H}_\mathrm{d}(\mathbf{r})$ and $\mathbf{M}(\mathbf{r})$ are parallel to the applied field. Then, from Eq. (2.16) we deduce that σ_M=0, so that $\mathbf{H}_\mathrm{d} = 0$ and $N_{\mathrm{f,m}} = 0$ from Eq. (2.36).

Many geometries of practical importance have clear principal directions, such as cylinders, rectangular prisms and ellipsoids, including all their limits. In chapter 3 we summarize the existing results for the demagnetizing factors for these geometries.

2.3 Hard superconductors

In this section we present an overview of some superconductor properties that are considered in the thesis. Readers are referred to Refs. [21, 22, 23] for deeper and more extended surveys on superconductivity.

2.3.1 Superconducting materials

Superconductors present a sharp resistivity decrease, when the material is cooled below some critical temperature T_c, to values several orders of magnitude lower than any conventional conducting material. When the material is placed below the critical temperature T_c we say that it is in the superconducting state, while if $T > T_\mathrm{c}$ it is in the normal state.

Another interesting property of superconductors is that below T_c they present flux quantization, that is, for any closed circuit inside a superconductor where there is no supercurrent, the magnetic flux over the surface bounded by the circuit must take an integer number of the flux quantum $\Phi_0 = h/2e$.

With regard to electromagnetic properties, we can distinguish between type I and type II superconductors.

Type I superconductors

If $T < T_\mathrm{c}$, type I superconductors keep $\mathbf{B} = 0$ inside its body for any applied magnetic field below a certain critical value H_c. Actually, there is a shell of depth λ

from the material border inwards where currents and magnetic induction are present[2]. A key issue is that if the cooling process to reach $T < T_c$ is done under a certain applied magnetic field, superconducting materials expulse the magnetic induction inside them. This effect is called Meissner effect.

A type I superconductor carrying a transport current only has nonzero current density in a layer of depth λ, since $\mu_0 \mathbf{J} = \nabla \times \mathbf{B}$ and $\mathbf{B} = 0$ in the bulk. The existence of the critical field H_c is the cause of the Silsbee effect, arising when the magnetic field created by a transport current in the surface of a superconducting wire equals to H_c. Then, normal regions appear in the superconductor and the wire resistivity becomes of the same order as in the normal state ([23], pp. 357-361). Since H_c is low and most of the cross-section of the wire does not carry current, type I superconductors are not practical for transport applications.

Type II superconductors

Type II superconductors have the same properties as type I for any applied field below a certain critical field $H_{c,1}$. However, between $H_{c,1}$ and another critical field $H_{c,2}$ ($H_{c,2} > H_{c,1}$), magnetic induction partially penetrate inside the material bulk in the form of superconducting current vortices containing flux inside them, forming the mixed state. These current vortices contains a flux quantum Φ_0 each, which is the minimum flux magnitude which can be surrounded by superconducting material. Under applied fields higher than $H_{c,2}$, superconductivity is suppressed.

Furthermore, type II superconductors with vortices present a resistive-like behavior when carrying a transport current. This effect is explained as follows. The transport current density $\mathbf{J}$ interacts to the current vortices, yielding to a driving force per unit length [24]

$$\mathbf{F}_d / L = \mathbf{J} \times \mathbf{\Phi}_0, \tag{2.43}$$

where the vector $\mathbf{\Phi}_0$ has magnitude Φ_0 and the same direction as the magnetic induction. This force makes the vortices move throughout the superconductor (flux flow), creating a local magnetic flux variation and, consequently, an induced electrical field $\mathbf{E}$. Then, ohmic loss $\mathbf{J} \cdot \mathbf{E}$ appears. We notice that the current vortices can appear as the result of either an external applied field or the self magnetic induction created by the transport current.

This ohmic loss appearing in ideal type II superconductors can be avoided under the presence of defects or impurities in the material. These defects or impurities can act as vortex pinning centers, that is, they can keep vortices fixed at a certain position. Then, if vortex density is not very high, pinning centers prevent flux motion and, consequently, ohmic loss. For this reason, defects and impurities are usually artificially created to improve type II superconductors practical properties. As it is explained in Sec. 2.3.3, these pinning centers allow nonzero vortex gradient density and, consequently, superconducting current inside the material bulk.

[2] Typical values of λ for type I superconductors range from 40 to 60 nm.

2.3.2 Currents and magnetization

Contrary to many magnetic materials, the magnetic moment created by a superconductor is due to free volume current density $\mathbf{J}$, which for type I superconductors with λ much lower than the sample dimensions can be approximately described as a sheet current density $\mathbf{K}$. This allows two possible descriptions of the magnetic properties.

First, the superconductor can be treated as a nonmagnetic material with free currents in it. With this description $\mathbf{M}(\mathbf{r}) = 0$ and $\mathbf{B} = \mu_0\mathbf{H}$, so that the physical role of the quantities $\mathbf{B}$ and $\mathbf{H}$ is the same.

The other possible description is to consider the current flowing into the superconductor as a magnetization current. Then, $\mathbf{J}_M = \nabla \times \mathbf{M}$ and $\mathbf{K}_M = \mathbf{M} \times \mathbf{e}_{\rm n}$, being $\mathbf{M}$ and effective local magnetization. This approach is useful for the perfect shielding state, which appears, for example, for type I superconductors with λ much lower than the sample dimensions. For this case the material can be taken as LHI with $\chi = -1$, so that $\mathbf{M} = -\mathbf{H}$ and $\mathbf{B} = 0$.

The latter description is used in Part I to discuss the demagnetizing effects in perfect shielding. However, the former approach is more practical (see below) for the critical-state model, since this model is based on an assumption of the critical current density $\mathbf{J}$. Nevertheless, for both approaches the magnetic induction is the same since its sources are $\mathbf{J}$ and $\mathbf{K}$, independently if they are considered as magnetization currents or not.

2.3.3 The critical-state model

The critical-state model was formulated to describe superconductors with strong pinning, also called hard superconductors.

Current vortices repeal to each other due to the force of Eq. (2.43), where in this case $\mathbf{J}$ is the current around one vortex. Then, the vortices natural behavior in an ideal type II superconductor is to uniformly distribute in average. For superconductors with impurities and lattice imperfections there appear pinning forces $\mathbf{F}_{\rm p}$, which attract the vortices to the impurity or imperfection position (pinning center). Pinning forces can compensate the vortices repulsion, allowing magnetic field gradients and, consequently, also nonzero macroscopic bulk current densities $\mathbf{J}$. Then, the magnitude of the bulk current is limited by the average maximum pinning force. Let name the magnitude of the maximum local bulk current density as $J_{\rm c}$.

Superconductors with strong pinning receive the name of *hard superconductors* because with increasing and then decreasing the applied field they present magnetization loops with high irreversibility. These superconductors also have high critical-current densities[3], which makes them very interesting for applications. Actually, hight-temperature superconductors and all superconducting materials with practical applications belong to the hard type.

The critical-state model, proposed by C. P. Bean and H. London [7, 8, 9], is based on

[3]Typical values of J_c in hard superconductors range between 10^5 and 10^7 A/cm^2.

the assumption that *any electromotive force, whatever small, will induce a macroscopic constant current*, J_c. This model applicability has been proved to be very broad to understand magnetic [7, 25, 26, 27, 28, 29, 17, 30, 31, 32, 33, 34] and transport [35, 36, 37, 38, 39, 40, 41, 42, 43] measurements in hard superconductors. The critical-state model implicitly assumes that $H_{c,1} = 0$ and neglects surface current effects, such as equilibrium magnetization or surface barriers. Although the original critical-state model assumed constant J_c, further extensions have been formulated for magnetic-induction-dependent J_c [44, 45, 46, 25, 47, 26], nonhomogeneous J_c [48, 49, 50] or anisotropic J_c [51].

As an example, we review in the following the original Bean-London model applied to an infinite slab. The main concepts reviewed here are useful for the development of chapters 6, 7 and 8.

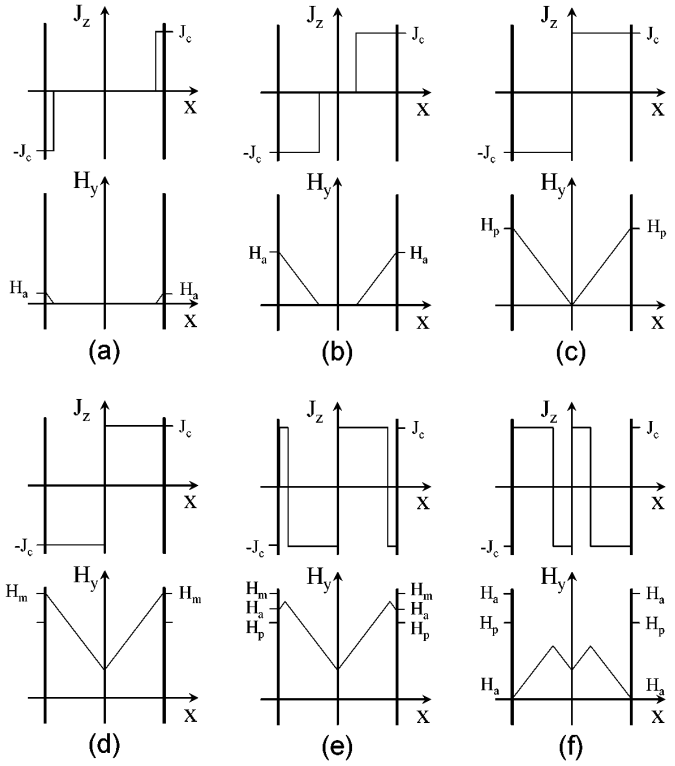

Figure 2.2: Sketch of current and field profiles in an infinite slab in longitudinal applied field H_a within the Bean's critical-state model.

We present for illustration the case of an infinite slab immersed in a uniform applied field H_a in an infinite direction starting from a zero-field cooled situation, that is, there is no magnetic field nor current density in the sample. If we gradually increase the magnetic field, some current density will be induced from the exterior to inwards following the Lenz law, Fig. 2.2. According to the main assumption of the model, this current density

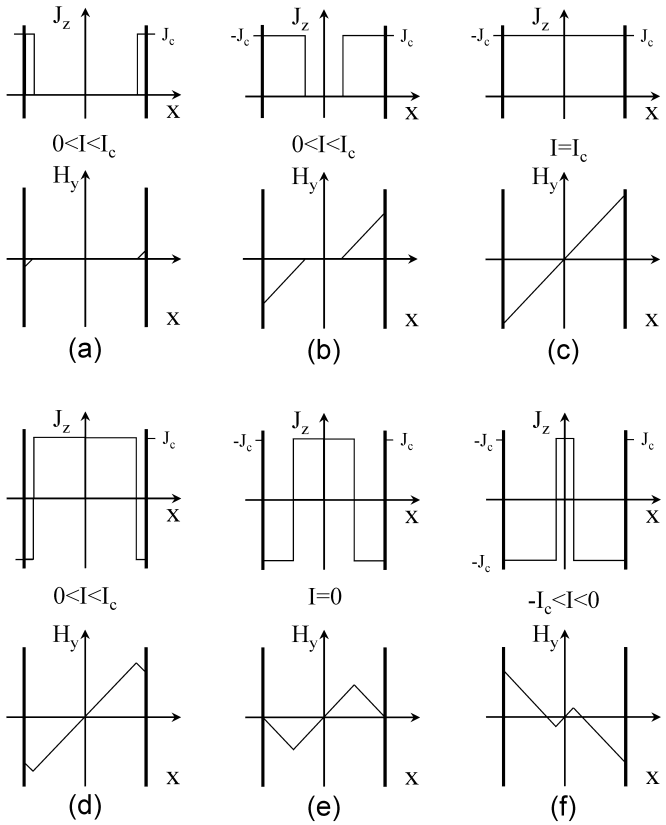

Figure 2.3: Sketch of current and field profiles in an infinite slab carrying transport current I within the Bean-London critical-state model.

have magnitude J_c [Fig. 2.2(a)]. Since $J_c = |\nabla \times \mathbf{H}| = |\partial H_y/\partial x|$, the magnetic field decreases linearly with slope J_c/μ_0 from the external value $H_y = H_a$ to 0 from the border to inside. Then, there can be distinguished a region with critical-current density and magnetic field and a field-free core with no current density [Fig. 2.2(a,b,c)]. With increasing the applied field, current density is induced inwards until the sample is fully penetrated [Fig. 2.2(c)]. The applied field at which this situation is reached receives the name of full penetration field H_p. Further increase in the applied field cannot induce more current, so that the inner magnetic field increases uniformly [Fig. 2.2(d)]. If the applied magnetic field is decreased after a maximum applied field H_m, the electromotive force induces current density in the opposite direction, having magnitude J_c. These currents, called reverse currents, penetrate in the same way as the initial ones and overlap the already existing current density. The previously set current density and magnetic field which are not overlapped by reverse ones are kept frozen [Fig. 2.2(d,e,f)].

We note that at low fields applied after the zero-field cooling state, the supercurrents shield this applied field in almost the whole volume of superconductor. Then, the perfect shielding approximation is suitable for this case and we can consider that the material

has an internal susceptibility $\chi = -1$.

The same process which has been presented for a uniform applied field can be repeated for a certain transport current I (Fig. 2.3). With increasing the transport current after a zero-field cooling, critical current and magnetic field penetrate from the exterior to inwards. The current at which the superconductor is penetrated is named critical current I_c. If the current is decreased after a maximum current $I_m \leq I_c$ is reached, reverse current penetrates from the surface inwards keeping the internal current density and magnetic field frozen. If, instead, the current is forced to be higher than I_c, the driving force on current vortices can no longer be compensated by pinning forces and ohmic loss appears in the superconductor.

The critical-state model has been extended to other geometries by many authors, as reviewed in the introduction of chapters 7 and 8. As it is mentioned in the introduction, this thesis provides an extension of the critical-state model for multifilamentary infinite superconducting samples with uniform transverse applied field or transport current.

Part I

Calculations of Demagnetizing Factors

CHAPTER 3

Introduction and numerical method

This part of thesis deals with the demagnetizing effects in some practical geometries, such as rectangular prisms and cylinders.

In this chapter we first review the state-of-the-art of demagnetizing calculations prior to our research. Afterwards, we present a numerical method to calculate the surface pole density and the demagnetizing factors for LHI materials with an arbitrary susceptibility. This method is described by means of a general formulation suitable for any geometry. Although the main part of our work on demagnetizing effects is based on numerical calculations using this method (see §4.2 and §5) [13, 52, 53], we also present some other relevant analytical results (see and §4.1) [54, 55].

3.1 Some interesting geometries

A complete review of the most interesting existing works on demagnetizing factors can be found in Refs. [3] and [56]. Here we present an overview of the existing results and some interesting features which are used in this thesis.

3.1.1 Ellipsoids

This geometry has great conceptual importance since it is the only one which presents uniform magnetization and demagnetizing field under a uniform applied magnetic field for any susceptibility χ [1]. As a consequence, the demagnetizing factors N_{f} and N_{m} defined in Eq. (2.36) are identical, so that a unique demagnetizing factor N needs to be considered. In addition, the demagnetizing factors are χ-independent, depending only on the relative length of the ellipse axes.

Thanks to the fact that the magnetization is uniform, an analytical expression of N can be obtained as a function of the elliptic integrals. The deduction of formulae for

N where derived in the beginning of the twentieth century and where systematically presented and summarized in 1945 by Osborn and Stoner [58, 57].

From the analytical result in [57, 58], it can be obtained that N for an ellipsoid with semiaxis a, b and c under an applied field in the c direction monotonically decrease when decreasing c with fixed a and b. Moreover, the limit of long samples, $c \gg a, b$, yields to $N \to 0$ while for short one, $c \ll a, b$, the limit is $N \to 1$. These qualitative results are fulfilled for any geometry.

3.1.2 Cylinders

This is a very interesting 3D geometry to calculate, since many actual magnetic samples have this shape. However, for this geometry no general analytical formulae can be obtained since the magnetization and the demagnetizing field are nonuniform for all $\chi \neq 0$.

The only case which can be analytically deduced is for $\chi = 0$ and axial applied field, for which the magnetization is uniform. As done by Joseph [59], the demagnetizing field can be calculated by direct integration considering that the pole density on the end surfaces is $\sigma = \pm M$ and null in the cylinder side. Then, the demagnetizing factors $N_{\mathrm{f,m}}$ are obtained by further integration of H_{d} over the midplane or the entire volume. An alternative deduction was made by Brown [60] by means of already existing formulae for mutual inductances. Thanks to Eq. (2.42) for uniform magnetization, the magnetometric demagnetizing factor in radial applied field, N_{m}^{r}, can be calculated from that corresponding to axial $\mathbf{H}_{\mathrm{a}}$, N_{m}^{a}, so that for the case $\chi = 0$

$$N_{\mathrm{m}}^{r}(\chi = 0) = \frac{1}{2}(1 - N_{\mathrm{m}}^{a}(\chi = 0)). \tag{3.1}$$

Although analytical solutions can only be deduced for $\chi = 0$, the demagnetizing factors for other susceptibilities can be calculated by using numerical methods. Many numerical methods are based on calculating first the surface pole density to obtain the demagnetizing field $\mathbf{H}_{\mathrm{d}}$ and the average magnetization $M_{\mathrm{mid,vol}}$ (§3.2) [3, 13, 52, 53]. For a cylinder with axial applied field, the system has rotational symmetry so that the problem can be mathematically reduced to a two dimensional one.

Considering 2D numerical calculations, it is worth to mention the accurate results obtained by Taylor in 1960 [61, 62] for N_{m} in either axial or radial applied fields, $\chi = -1$ and ∞, and lenght-to-diameter ratio in $0.25 \leq \gamma \leq 4$. Afterwards, quite accurate calculations of axial N_{f} for a wider range of γ and χ were made under the help of computers [2, 4], and the γ and χ dependence of the axial $N_{\mathrm{f,m}}$ was practically completed and discussed for cylinders in [3, 63]. Calculations for radial $N_{\mathrm{f,m}}$ are more incomplete, being N_{f} calculated for $\chi > 0$ and $0.01 \leq \gamma \leq 100$ in [5] and N_{m} for $-1 \leq \chi \leq 10^{9}$ and $0.01 \leq \gamma \leq 1$ in [55].

From the analytical results for ellipsoids and cylinders with $\chi = 0$ in axial field, we can do a comparison between the demagnetizing factors for cylinders with diameter D and length L and ellipsoids with semiaxis a, a, c so that $\gamma \equiv L/D = c/a$. When

doing so, the demagnetizing factors differ in more than 10% for γ between 0.1 and 0.5, a difference that can be higher than 100% for a γ larger than 2. This difference exemplifies the significant dependence of the demagnetizing factors on the sample shape and the importance of their calculation for any practical geometry.

3.1.3 Rectangular prisms

The rectangular prism geometry has great practical importance. For this reason, a lot of effort has been made to obtain the demagnetizing factors for this geometry, both numerically and analytically. Two separate cases must be considered: infinitely long prisms (bars) and finite ones. As explained in §2.2.2, the demagnetizing factors $N_{\mathrm{f,m}}$ for the infinite directions are null, so that for the infinitely long prisms only the transverse demagnetizing factors have to be calculated. The case of infinitely long prisms is easier to solve due to the translational symmetry in the infinite direction, thanks to which the problem is reduced to a two dimensional one.

Infinite rectangular prisms

For infinite bars exact analytical formulae can be derived for $\chi = 0$, -1 and ∞. In 1960's Brown presented a comprehensive work on analytical formulae for infinite prisms. He calculated $N_{\mathrm{f,m}}$ for uniform magnetization by means of direct integration (appendix in [18]). Furthermore, he also calculated the analytical solution for $\chi = \infty$ by means of conformal mapping thanks to the analogy with the electrical field in a conductor, in the sense that for infinite susceptibility $\mathbf{H}$ is null inside the magnetic sample, while for a conductor the electric field vanishes [18]. However, Brown never published the specific deduction nor the surface pole density σ. Recently, Brandt and Mikitik analytically obtained χ^{ext} for $\chi = -1$ [64], from which N_{m} can be deduced by means of Eq. (2.37). Although Brandt and Mikitik mention in their article that they use conformal mapping, the do not specify the process to calculate the sheet currents, from which χ^{ext} is calculated. We deduced the demagnetizing factors $N_{\mathrm{f,m}}$ for $\chi = -1$ from solving step by step the $\chi = \infty$ case and using a conjugate relations between $\chi = \infty$ and $\chi = -1$ [54, 65]. Apart from $N_{\mathrm{f,m}}$ analytical formulae and tables, in that article we calculated the surface pole density σ for $\chi = \infty$ and the sheet current $\mathbf{K}_M$ for $\chi = -1$. The main results and the method used for these susceptibilities are summarized in Sec. 4.1.

Apart from the above analytical results for $\chi = 0$, ∞ and -1, there exist neither analytical results nor numerical ones for any other susceptibility values. In order to fill this lack, we numerically calculated $N_{\mathrm{f,m}}$ for a wide susceptibility range [13]. The numerical method used to calculate them is presented in a general formulation in §3.2 and the results obtained are summarized in §4.2.

Finite rectangular prisms

For finite rectangular prisms there only exist analytical solutions for uniform magnetization, that is, $\chi = 0$. The magnetometric demagnetizing factor was first calculated by Rhodes and Rowlands [66] in 1954 by energy considerations [66], while later Joseph published analytical formulae for both N_{f} and N_{m} obtained by direct integration. The specific case of N_{m} for a cube with uniform magnetization can be easily calculated from Eq. (2.42) yielding to $N_{\mathrm{m}} = 1/3$, which is the same as for a sphere.

Apart from the analytical results for uniform magnetization, the only existing results for finite rectangular prisms are the N_{f} numerical calculations for square bars obtained by Templeton and Arrot for $\chi = \infty$ and a wide range of length-to-side aspect ratio [2]. Templeton and Arrot results for square bars can be compared to those for cylinders, also obtained in [2], which show that N_{f} for a square bar and a cylinder with same length and cross-section only differ between 1.5% and 3%. Similar results are obtained for χ^{ext}, directly related to N_{m}, for perfectly shielded rectangular bars ($\chi = -1$) obtaining a difference of 1% for a length-to-semiside ratio of 10 up to 5% for a ratio of 0.1 [67].

In this thesis we present numerical calculations of the demagnetizing factors $N_{\mathrm{f,m}}$ for finite square and rectangular prisms in chapter 5, which can also be found in [52, 53]. The numerical calculation of the demagnetizing factors for finite rectangular prisms is much more complicated than for infinitely long rectangular prisms, since the change from 2D problems to 3D implies much more than 50% of computation time and memory. As explained below, this fact motivated the refinement of the method previously used for infinite rectangular prisms and cylinders [13, 3].

We next present the general numerical method used to calculate the surface pole density and the fluxmetric and magnetometric demagnetizing factors for arbitrary susceptibility and a wide range or samples dimensions. As mentioned above, this numerical method has been applied to cylinders [3], infinite rectangular bars [13] and finite square and rectangular bars [52, 53]. In the research work of this thesis we adapted the original method presented in [3] for cylinders to infinite rectangular prisms and improved it to make the method applicable to rectangular bars, obtaining for both geometries highly accurate results.

3.2 Numerical method for arbitrary susceptibility

As explained in the previous section, the determination of the demagnetizing factors for arbitrary susceptibility requires numerical calculations, even for regular geometries such as cylinders and rectangular prisms. In this section we present a general numerical method to calculate the demagnetizing factor for a LHI sample, based on that developed by Chen, Brug and Goldfarb [3].

As mentioned in §2.2.2, the calculation of the demagnetizing factors $N_{\mathrm{f,m}}$ in a LHI material requires either $M_{\mathrm{mid,vol}}$, $H_{\mathrm{d,mid,vol}}$ or $B_{M,\mathrm{mid,vol}}$, so that $N_{\mathrm{f,m}}$ can be obtained by means of Eqs. (2.39), (2.40) or (2.41), respectively. By definition, the demagnetizing

field $\mathbf{H}_\mathrm{d}$ can be calculated by direct integration from σ_M, while $\mathbf{B}_M$ is calculated from the magnetization sheet current $\mathbf{K}_M$.

The numerical method developed in this thesis requires the division of the sample surface into elements, in each of which σ_M or $\mathbf{K}_M$ is uniform. After doing so, the σ_M or $\mathbf{K}_M$ values on the elements are calculated by solving a linear equation system. From the surface pole density or the magnetization sheet current, the quantities $\mathbf{H}_\mathrm{d}$ or $\mathbf{B}_M$ are obtained, respectively, which the demagnetizing factors can be calculated from.

Although in principle the demagnetizing factors can be calculated from either σ_M or $\mathbf{K}_M$, the use of $\mathbf{K}_M$ for finite rectangular prisms requires a double number of independent variables than using σ_M, due to the vectorial nature of the sheet currents. Consequently, considering that the algorithm used to solve the linear equation system has a temporal complexity of n^3, being n the number of independent variables, the use of $\mathbf{K}_M$ requires eight times more computational time than using σ_M.

Furthermore, Chen, Brug and Goldfarb provided a useful correction to reduce the discretization error (Eq. (40b) in [3]). As explained below, in some cases this correction can reduce the discretization error in several orders of magnitude. This correction requires the calculation of the demagnetizing factors from both $M_\mathrm{mid,vol}$ and $H_\mathrm{d,mid,vol}$. The mean magnetization can be calculated from σ_M thanks to $\nabla\cdot\mathbf{M}=0$ (§3.2.2) [3, 54], which cannot be done from $\mathbf{K}_M$.

3.2.1 Surface pole density calculation

In order to obtain $N_\mathrm{f,m}$ we need to calculate first the surface pole density σ_M on the sample surface. We now describe a general numerical method which can, in principle, be applied to any geometry. From now on, we will omit the subindex 'M' to simplify the notation.

For a LHI material, the local magnetization is proportional to the magnetic field, $\mathbf{M}=\chi\mathbf{H}$. Considering the component perpendicular to the surface and the σ definition of Eq. (2.18), we obtain

$$\sigma(\mathbf{r}) = \chi\left[\mathbf{H}_\mathrm{a}(\mathbf{r}) + \mathbf{H}_\mathrm{d}(\mathbf{r})\right]\cdot\mathbf{e}_\mathrm{n}(\mathbf{r}), \tag{3.2}$$

where $\mathbf{e}_\mathrm{n}(\mathbf{r})$ is the unit vector perpendicular to the surface at position $\mathbf{r}$. In Eq. (3.2) we allow the general case of a nonuniform applied field, although in this thesis we only consider uniform applied fields. Then, we divide the surface into n elements where we assume a uniform pole density. The error due to this approximation decreases with increasing the number of elements n. Considering this approximation, the demagnetizing field at position $\mathbf{r}$ is

$$\mathbf{H}_\mathrm{d}(\mathbf{r}) = \sum_j \sigma^j \mathbf{h}^j(\mathbf{r}) \tag{3.3}$$

where σ^j is the surface pole density at element j and $\mathbf{h}^j(\mathbf{r})$ is the magnetic field for unit

pole density created by this element, so that

$$\mathbf{h}^j(\mathbf{r}) \equiv \frac{1}{4\pi} \int_{S_j} \mathrm{d}S' \frac{\mathbf{r} - \mathbf{r}'}{|\mathbf{r} - \mathbf{r}'|^3} \tag{3.4}$$

with S_j as the element j cross-section. From Eqs. (3.2) and (3.4) we obtain the linear equations set

$$H^i_{\mathrm{a,n}} = \sum_j \left(\frac{\delta^{ij}}{\chi} + N^{ij}_{\mathrm{n}} \right) \sigma^j, \tag{3.5}$$

where δ^{ij} is the Kronecker symbol and $H^i_{\mathrm{a,n}}$ and N^{ij}_{n} are defined as $H^i_{\mathrm{a,n}} \equiv \mathbf{H}_{\mathrm{a}}(\mathbf{r}^i) \cdot \mathbf{e}_{\mathrm{n}}(\mathbf{r}^i)$ and $N^{ij}_{\mathrm{n}} \equiv -\mathbf{h}^j(\mathbf{r}^i) \cdot \mathbf{e}_{\mathrm{n}}(\mathbf{r}^i)$, being $\mathbf{r}^i$ the element i central position.

For a given applied field $\mathbf{H}_{\mathrm{a}}$ and knowing the geometrical coefficients N^{ij}_{n}, the surface pole density at each element σ^i can be calculated by solving the linear equation set (3.5). Actually, this linear equation set is only useful to calculate the surface pole density provided that the coefficients $\mathbf{h}^j(\mathbf{r})$ can be calculated analytically by means of Eq. (3.4). This method has been used for cylinders and infinite rectangular prisms [3, 13].

The numerical method presented above can be improved by considering the average demagnetizing field on the element surface, instead of $\mathbf{H}_{\mathrm{d}}$ in the center only. When doing so, the linear equation system for σ^i changes into

$$H'^i_{\mathrm{a,n}} = \sum_j \left(\frac{\delta^{ij}}{\chi} + D^{ij}_{\mathrm{n}} \right) \sigma^j, \tag{3.6}$$

where $H'^i_{\mathrm{a,n}}$ is the average of $\mathbf{H}_{\mathrm{a}}(\mathbf{r}) \cdot \mathbf{e}_{\mathrm{n}}(\mathbf{r})$ on the element i surface and D^{ij}_{n} is defined as

$$D^{ij}_{\mathrm{n}} \equiv -\int_{S_i} \mathrm{d}S \mathbf{e}_{\mathrm{n}}(\mathbf{r}) \cdot \mathbf{h}^j(\mathbf{r}). \tag{3.7}$$

We apply this latter method to rectangular prisms [52, 53], showing a much higher accuracy in the surface pole density than when considering the demagnetizing field in the element center only. However, in order to apply the linear equation set of Eq. (3.6) we need the analytical expression for D^{ij}_{n}, which can be calculated from Eq. (3.7) by direct integration of $\mathbf{h}^j(\mathbf{r})$. The calculation of D^{ij}_{n} requires an extra integration compared to N^{ij}_{n}, so that for some geometries only N^{ij}_{n} have an analytical expression but not D^{ij}_{n}, as is the case for cylinders.

3.2.2 Calculation of the demagnetizing factors

Once the surface pole distribution is known, we can calculate $M_{\mathrm{mid,vol}}$ and $H_{\mathrm{d,mid,vol}}$, from which the demagnetizing factors $N_{\mathrm{f,m}}$ can be calculated using Eqs. (2.39) and (2.40), respectively. As mentioned above, the demagnetizing factors are calculated by two different methods in order to use a $N_{\mathrm{f,m}}$ correction, which significantly reduces the discretization error [3].

Let us take the uniform applied field $\mathbf{H}_\mathrm{a}$ to be in the z direction with the origin located in the center of the sample. If the sample geometry has mirror symmetry in the xy plane, both $\mathbf{M}_\mathrm{mid,vol}$ and $\mathbf{H}_\mathrm{d,mid,vol}$ are in the z direction, §2.2.1, so that we can ignore the vector nature of these quantities.

Average magnetization calculation

The average magnetization on any surface with constant z, $M_\mathrm{av}(z)$, can be calculated from σ thanks to $\nabla \cdot \mathbf{M} = 0$, which is fulfilled for any LHI material. From $\nabla \cdot \mathbf{M} = 0$ it can be deduced that the integral $\oint \mathbf{M} \cdot \mathrm{d}\mathbf{s}$ is null on any surface closing a volume inside the magnetic sample. Then, $M_\mathrm{av}(z)$ is

$$M_\mathrm{av}(z) = \frac{1}{S(z)} \int_{S(z' \geq z)} \mathrm{d}S' \sigma(\mathbf{r}'), \tag{3.8}$$

where $S(z)$ is the sample cross-section at height z and $S(z' \geq z)$ is the sample surface above z. Then,

$$M_\mathrm{mid} = M_\mathrm{av}(z = 0), \tag{3.9}$$

$$M_\mathrm{vol} = (1/l) \int_0^l M_\mathrm{av}(z)\mathrm{d}z, \tag{3.10}$$

being $2l$ the sample length. For obtaining the above formula for M_vol we have used the sample mirror symmetry with respect to the $y = 0$ plane.

Average demagnetizing field calculation

The average demagnetizing fields $H_\mathrm{d,mid}$ and $H_\mathrm{d,vol}$ are

$$H_\mathrm{d,mid} = \frac{1}{S_\mathrm{mid}} \int_{S_\mathrm{mid}} \mathrm{d}S H_{\mathrm{d},z}(\mathbf{r}) = \sum_j \sigma^j h^j_{z,\mathrm{mid}}, \tag{3.11}$$

$$H_\mathrm{d,vol} = \frac{1}{V} \int_V \mathrm{d}V H_{\mathrm{d},z}(\mathbf{r}) = \sum_j \sigma^j h^j_{z,\mathrm{vol}}, \tag{3.12}$$

where the factors $h^j_{z,\mathrm{mid}}$ and $h^j_{z,\mathrm{vol}}$ are the element j contribution to $H_\mathrm{d,mid,vol}$ normalized to σ^j, respectively. Naturally, the analytical obtention of factors $h^j_{z,\mathrm{mid}}$ and $h^j_{z,\mathrm{vol}}$ is preferred than any numerical evaluation. Again, this analytical derivation is not possible for cylinders, so that a surface or volume numerical integration of $H_{\mathrm{d},z}(\mathbf{r})$ from Eq. (3.3) is needed. We note that the use of analytical formulae for $h^j_{z,\mathrm{mid}}$ and $h^j_{z,\mathrm{vol}}$ improves significantly both the accuracy and the computation time of $H_\mathrm{d,mid,vol}$ from the numerical σ solution [52].

Demagnetizing factors calculation

Once $M_\mathrm{mid,vol}$ and $H_\mathrm{d,mid,vol}$ are obtained, the demagnetizing factors $N_\mathrm{f,m}$ can be calculated from Eqs. (2.39) and (2.40). Although the demagnetizing factors calculated

from both equations should yield the same value, it is not so due to the discretization error in σ. To distinguish between the $N_{\mathrm{f,m}}$ values obtained from the different equations, we name the demagnetizing factors obtained from $M_{\mathrm{mid,vol}}$ as the surface demagnetizing factors, $N^s_{\mathrm{f,m}}$, and those obtained from $H_{\mathrm{d,mid,vol}}$, as volume demagnetizing factors $N^v_{\mathrm{f,m}}$.

As explained in [3], a corrected demagnetizing factor value $N^c_{\mathrm{f,m}}$ can be obtained from $N^s_{\mathrm{f,m}}$ and $N^v_{\mathrm{f,m}}$ using

$$N^c_{\mathrm{f,m}} = N^v_{\mathrm{f,m}} \frac{1 + N^s_{\mathrm{f,m}}\chi}{1 + N^v_{\mathrm{f,m}}\chi}. \tag{3.13}$$

This relation can be obtained from Eqs. (2.39) and (2.40) assuming that the relative error in $M_{\mathrm{mid,vol}}$ and $H_{\mathrm{d,mid,vol}}$ are the same. This last assumption is formulated as

$$\delta_{\mathrm{mid,vol}} = 1 - \frac{M_{\mathrm{mid,vol}}}{M^*_{\mathrm{mid,vol}}} = 1 - \frac{H_{\mathrm{d,mid,vol}}}{H^*_{\mathrm{d,mid,vol}}}, \tag{3.14}$$

where $\delta_{\mathrm{mid,vol}}$ is the relative error and $M^*_{\mathrm{mid,vol}}$ and $H^*_{\mathrm{d,mid,vol}}$ are the correct ideal values of $M_{\mathrm{mid,vol}}$ and $H_{\mathrm{d,mid,vol}}$, respectively.

3.3 On $N_{\mathrm{f,m}}$ and $1 - N_{\mathrm{f,m}}$

We now present some general considerations upon $N_{\mathrm{f,m}}$ and its relation to $M_{\mathrm{mid,vol}}$, which is the quantity that is desired to determine when doing fluxmetric and magnetometric measurements (§2.2.2). These considerations are useful when discussing the error of numerical calculations [13].

In a similar way in which we have defined the external susceptibility χ^{ext} in Sec. 2.1.3, we can define $\chi_{\mathrm{ext,mid,vol}}$ as

$$\chi^{\mathrm{ext}}_{\mathrm{mid,vol}} \equiv M_{\mathrm{mid,vol}}/H_{\mathrm{a}}. \tag{3.15}$$

These external susceptibilities are related to demagnetizing factors as

$$\chi^{\mathrm{ext}}_{\mathrm{mid,vol}} = \frac{1}{N_{\mathrm{f,m}} + 1/\chi}. \tag{3.16}$$

The magnetic materials and their demagnetizing factors study has traditionally been done for magnetic materials with high susceptibility, $\chi \gg 1$.

The relevant quantity for materials with $\chi \gg 1$ is the shape susceptibility χ_s, defined as

$$\chi_s = \chi^{\mathrm{ext}}_{\mathrm{mid,vol}}(\chi = \infty) = 1/N_{\mathrm{f,m}}. \tag{3.17}$$

Actually, this χ_s is defined at one extreme value of χ, and if using the other extreme value $\chi = -1$, we will have another shape susceptibility

$$\chi^*_s = \chi^{\mathrm{ext}}_{\mathrm{mid,vol}}(\chi = -1) = -1/(1 - N_{\mathrm{f,m}}). \tag{3.18}$$

In the first case, what determines the accuracy of χ_s is the accuracy of $N_{\mathrm{f,m}}$; in the second case, the accuracy of χ^*_s is determined by that of $1 - N_{\mathrm{f,m}}$. Thus, the accuracy

of $N_{\mathrm{f,m}}$ determination should be required with respect to $N_{\mathrm{f,m}}$ itself if $\chi \gg 1$ and to $1 - N_{\mathrm{f,m}}$ if $\chi \approx -1$. Related to this, when making the error estimations at any value of χ, we will more strictly define the relative error of the demagnetizing factors as the higher one obtained from $N_{\mathrm{f,m}}$ or $1 - N_{\mathrm{f,m}}$.

3.4 Chapter summary and conclusions

Since the definition of the demagnetizing factors, which was contemporary to Maxwell himself [1], a lot of work has been done to calculate them. Some of this work is reviewed in this chapter. From the published results, it can be found that the demagnetizing factors $N_{\mathrm{f,m}}$ can strongly depend on the sample geometry. Then, $N_{\mathrm{f,m}}$ must be calculated independently for each interesting geometry. We have detected some lacks in the demagnetizing factors published results even for the regular geometries of cylinders and rectangular prisms. Although there can be some others, these lacks are overviewed below.

For infinitely long prisms, there exist only some results for particular values of susceptibility $\chi = -1, 0, \infty$, which are found analytically. Although for $\chi = \infty$ both the fluxmetric and magnetometric demagnetizing factors are calculated, neither their deduction nor the surface pole density σ have been published. For $\chi = -1$ only N_{m} has been obtained. Furthermore, there are no $N_{\mathrm{f,m}}$ results for intermediate values of χ, which can only be calculated numerically.

There are even less results for the general case of a finite rectangular prism. Actually, the only analytical results are for $\chi = 0$ and there are only some numerical calculations for N_{f} and $\chi = \infty$.

At least part of these lacks in $N_{\mathrm{f,m}}$ results can be covered by appropriate numerical calculations. For this reason we present in this chapter a general formulation of a numerical procedure which was first developed for cylinders in axial applied field [3]. Furthermore, we improve this method by considering analytical formulae for surface and volume averages.

CHAPTER 4

Infinitely long rectangular bars in transverse field

In this chapter we present the main demagnetizing effects results for samples with the geometry of infinitely long rectangular bars. Although the study of this geometry has some practical interest, specially for $\chi = -1$, the study of infinitely long rectangular strips must be taken as a step to solve the more interesting finite prisms geometry.

Although the numerical model presented in §3.2 is valid for any physical susceptibility, for some χ values, $\chi = -1, 0, \infty$, it is possible to deduce analytical formulae for the demagnetizing factors and the surface pole density σ or the magnetization sheet current $\mathbf{K}_M$. As it is explained below (§4.2.3), the error in the numerical calculations can be checked by comparison to the derived exact analytical formulae. The deduction of these formulae requires the use of relations between the magnetometric demagnetizing factors of different strips, which we call the conjugate relations (§4.1.1). Similar conjugate relations, although approximate, can be found for other geometries, such as cylinders and cubes. These conjugate relations for cylinders can be used for approximate calculations of the radial magnetometric demagnetizing factor from the previous results of the axial one.

After presenting the analytical results, we expose the numerical ones for arbitrary χ obtained from the method described in Sec. 3.2 adapted to the infinite rectangular prism geometry. To make this adaptation, the analytical formulae for σ with $\chi = \infty$ and $N_{\mathrm{f,m}}$ with $\chi = -1, 0$ and ∞ have been of fundamental importance for estimating and reducing the discretization error.

4.1 Exact analytical calculations for extreme values of susceptibility

In this section we outline the main analytical results for $\chi = -1$ and ∞, published in Ref. [54] and detailed in Ref. [65]. Although, the analytical formulae for $N_{\mathrm{f,m}}$ with $\chi = \infty$ and for N_{m} with $\chi = -1$ were already published[1], in Refs. [54, 65] we not only presented all the steps to obtain the demagnetizing factors but also calculated the surface pole density σ for $\chi = \infty$, which did not appear in the original results.

We will start by presenting some relations, which we call conjugate relations, relating demagnetizing properties between samples with same dimensions but different susceptibility. Thanks to these relations, we can obtain $\mathbf{K}_M$ and N_{m} for $\chi = -1$ from the σ and N_{m} results for $\chi = \infty$, respectively.

4.1.1 Conjugate relations for infinitely long rectangular prisms

In this subsection we focus on infinitely long rectangular prism of dimensions $2a \times 2b$ in the x and y directions, respectively, having its infinite dimension parallel to the z axis (Fig. 4.1). We assume that there are no free currents in the sample ($\mathbf{J} = \mathbf{K} = 0$). Then, since for LHI materials the magnetization current density $\mathbf{J}_M$ and the volume pole density ρ_M are always zero (§2.1.3), the only sources for vector potential $\mathbf{A}$ and magnetic scalar potential ϕ are $\mathbf{K}_M$ and σ, respectively. Moreover, for applied fields in the xy plane, the sheet current $\mathbf{K}_M$ flows in the z direction. Since the vector potential in the Coulomb gauge ($\nabla \cdot \mathbf{A} = 0$) is

$$\mathbf{A}(\mathbf{r}) = \frac{\mu_0}{4\pi} \int_S \frac{\mathbf{K}_M(\mathbf{r}')}{|\mathbf{r} - \mathbf{r}'|} \mathrm{d}^2\mathbf{r}', \tag{4.1}$$

the vector potential is parallel to the z direction. In addition, neither $\mathbf{A}$ nor ϕ depend on the z position thanks to the translational symmetry.

We consider now an infinite prism with susceptibility χ_1 immersed in an applied field in the x direction (prism 1) and another one with susceptibility χ_2 and the same applied field but in the y direction (prism 2), Fig. 4.1.

In Ref. [54] we demonstrated that as long as the condition

$$\frac{\mu_{i,1}}{\mu_0} = \frac{\mu_0}{\mu_{i,2}} \tag{4.2}$$

is fulfilled, the scalar magnetic potential for prism 1, ϕ_1, and the z component of the vector potential for prism 2, A_2, divided by μ_0, follow the same differential equations with the same boundary conditions. This issue can be deduced from the $\mathbf{A}$ and ϕ differential equations and boundary conditions of section §2.1.3. Consequently ϕ_1 is proportional to A_2,

$$\phi_1(x, y) = A_2(x, y)/\mu_0. \tag{4.3}$$

[1] The demagnetizing factors $N_{\mathrm{f,m}}$ for $\chi = \infty$ were calculated by Brown [18] and Brandt and Mikitik presented a formula for χ^{ext} for $\chi = -1$ [64], from which N_{m} can be directly deduced by means of Eq. (2.37).

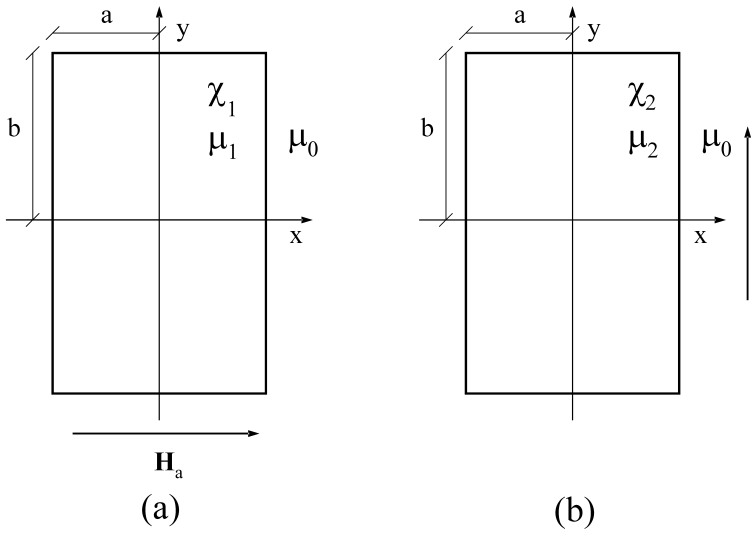

Figure 4.1: Infinite prism cross-section of dimensions $2a \times 2b$ under an applied field of magnitude $H_{\rm a}$ in the x (a) and y (b) directions. The prism is a LHI magnetic material with susceptibility χ_1 (a) and χ_2 (b), respectively.

The permeability condition of Eq. (4.2) is equivalent to the following susceptibility one

$$\chi_1 = \chi^*, \tag{4.4}$$

$$\chi_2 = -\frac{\chi^*}{1+\chi^*}, \tag{4.5}$$

being χ^* any number between -1 and ∞.

Equation (4.3) has some important implications. From Eq. (2.8) and (2.16) and taking into account that $\mathbf{H} = -\nabla\phi$ and $\mathbf{B} = \nabla \times \mathbf{A}$ we deduce that

$$\sigma = \nabla\phi \cdot \mathbf{e}_{\rm n}, \tag{4.6}$$

$$\mathbf{K}_M = \frac{1}{\mu_0} (\nabla A \cdot \mathbf{e}_{\rm n})\, \mathbf{e}_z, \tag{4.7}$$

where the second equation is obtained by using $\nabla \times \mathbf{A} = \nabla A \times \mathbf{e}_z$ for the infinitely long geometry. Then, Eq. (4.3) implies that

$$\sigma_1(x, y; \chi = \chi^*) = K_{2,M}(x, y; \chi = -\chi^*/(1+\chi^*)), \tag{4.8}$$

where the subindices 1 and 2 refer to prism 1 and 2, respectively. If one wants to study the infinitely long prism geometry with an applied field always in the same direction, we can rotate prism 2 axis anti-clockwise a $\pi/2$ angle, Fig. 4.1(b). Moreover, the prism semisides should be renamed so that the prism vertical dimension is $2a$ and the horizontal one is $2b$. After doing these changes Eq. (4.8) becomes

$$K'_M\,(x, y; a/b; \chi = -\chi^*/(1+\chi^*)) = \sigma_M(-y, x; b/a; \chi = \chi^*), \tag{4.9}$$

where K'_M is the sheet current for the rotated prism 2.

We next present the conjugate relation for $M_{\rm vol}$ between the prisms. For prism 2 we can use the dipolar magnetic moment definition[2], while for prism 1 the electric dipolar moment formulae can be applied. Then, we obtain

$$M_{\rm vol,1} = \frac{1}{ab}\left[a\int_0^b \sigma(a,y)\mathrm{d}y + \int_0^a x\sigma(x,b)\mathrm{d}x\right] \tag{4.10}$$

$$M_{\rm vol,2} = -\frac{1}{ab}\left[a\int_0^b K_M(a,y)\mathrm{d}y + \int_0^a xK_M(x,b)\mathrm{d}x\right]. \tag{4.11}$$

Consequently, since $K_{M,2} = \sigma_1$ the volume average magnetization follows the relation

$$M_{\rm vol,1} = -M_{\rm vol,2}. \tag{4.12}$$

Considering that $\mathbf{M} = \chi\mathbf{H}$ and by means of Eqs. (4.12), (2.36) and (2.32) the following relation between the magnetometric demagnetizing factor can be deduced

$$N_{\rm m,1} + N_{\rm m,2} = 1, \tag{4.13}$$

where $N_{\rm m,1}$ and $N_{\rm m,1}$ are the magnetometric demagnetizing factors for prism 1 and 2, respectively, in Fig. 4.1. As done above for σ and K_M, we can rotate prism 2 and the applied field if Fig. 4.1(b) so that $\mathbf{H}_{\rm a}$ is parallel to the x direction. Then, the demagnetizing factors for rectangular prisms with applied field in the x direction follow the relation

$$N_{\rm m}(a/b,\chi^*) + N_{\rm m}(b/a,\frac{-\chi^*}{1+\chi^*}) = 1. \tag{4.14}$$

This last conjugate relation, Eq. (4.14), is of great importance for the calculations for the infinitely long geometry, since the $N_{\rm m}$ results for a certain susceptibility χ^* for a range of a/b can be directly used to obtain those for susceptibility $-\chi^*/(1+\chi^*)$. In particular, thanks to Eq. (4.14), the $N_{\rm m}$ values for $\chi = -1$ can be obtained from the analytical formulae for $\chi = \infty$ published by Brown [18] and rederived in [54, 65].

Conjugate relations for other geometries

It is possible to find some other conjugate relations for other geometries, although they are not as general as for infinite strips.

For cylinders, we can deduce a conjugate relation for $N_{\rm m}$ similar to Eq. (4.14). This relation is

$$N^a_{\rm m}(R/l,\chi=\chi^*) + 2N^r_{\rm m}(R/l,\chi=-\chi^*/(1+\chi^*)) = 1+\delta(R/l,\chi^*), \tag{4.15}$$

where R is the cylinder radius, $2l$ its length, $N^a_{\rm m}$ and $N^r_{\rm m}$ are the magnetometric demagnetizing factors in the axial and radial directions, respectively, and $\delta(R/l,\chi^*)$ is a factor

[2]For the infinitely long geometry approximation, the currents of the U-turn at the far-away ends of the sample give the same contribution to $\mathbf{m}$ as the currents in a cross-section, thus canceling the factor 1/2 in the $\mathbf{m}$ definition of Eq. (2.1) [87].

that accounts for the deviation from 1 of the conjugate relation. It can be proved that $\delta(R/l, \chi^*) = 0$ for $\chi^* = -1$ and 0, so that we obtain a relation similar to Eq. (4.14)[55]. In Ref. [55, 65] we estimate the factor $\delta(R/l, \chi^*)$ for cylinders with $R/l \leq 1$ and we use this estimation to calculate the radial magnetometric demagnetizing factors N_{m}^r from the numerical results in [3]. The maximum estimated discretization error for these N_{m}^r values is of about 1%.

From the numerical N_{m} results for a cube, presented in Sec. 5.2.3 and in [52], we can find a similar conjugate relation, Eq. 5.1.

4.1.2 Infinitely long prism with infinite susceptibility

We now present the main analytical results obtained for $\chi = \infty$. The surface pole density σ on the prism is obtained by solving the magnetic scalar potential for an infinite cylinder with the same susceptibility and applied field and transforming the external region for a circle into that for a rectangle by means of conformal mapping transformations. Once the surface pole density is obtained, the calculation of the demagnetizing factors can be done by direct integration. The details of the deduction of σ and $N_{\mathrm{f,m}}$ can be found in [54, 65].

Surface pole density

After doing the appropriate conformal transformation, the surface pole density on a prism with $\chi = \infty$ with orientation like in Fig. 4.1 is found as

$$\sigma(a, y) = \frac{H_{\mathrm{a}} \cos\theta}{\sqrt{k^2 - \sin^2\theta}} \qquad (0 \leq \theta \leq \arcsin k), \tag{4.16}$$

$$\sigma(x, b) = \frac{H_{\mathrm{a}} \cos\theta}{\sqrt{\sin^2\theta - k^2}} \qquad (\arcsin k \leq \theta \leq \pi/2), \tag{4.17}$$

where the parameter k is related to a, b and a/b as

$$a = 2[E(k') - k^2 K(k')], \tag{4.18}$$

$$b = 2[E(k) - k'^2 K(k)], \tag{4.19}$$

$$\frac{a}{b} = \frac{E(k') - k^2 K(k')}{E(k) - k'^2 K(k)}. \tag{4.20}$$

with $k'^2 = 1 - k^2$ and $K(k)$ and $E(k)$ as the complete elliptical integrals of the first and second kind, respectively. The angle θ in Eqs. (4.16) and (4.17) is related to the coordinates x and y by means of

$$\frac{y}{b} = \frac{E(\vartheta, k) - k'^2 F(\vartheta, k)}{E(k) - k'^2 K(k)}, \tag{4.21}$$

$$\frac{x}{a} = \frac{E(\vartheta', k') - k^2 F(\vartheta', k')}{E(k') - k^2 K(k')}, \tag{4.22}$$

where $E(\vartheta, k)$ and $F(\vartheta, k)$ are the first and second kind elliptical integrals, and ϑ and ϑ' are defined as

$$\sin\vartheta = \sin\theta/k \qquad (0 \le \theta \le \arcsin k), \tag{4.23}$$

$$\sin\vartheta' = \sin\theta'/k' = \sin(\pi/2-\theta)/k' \qquad (\arcsin k \le \theta \le \pi/2). \tag{4.24}$$

The pole density $\sigma(a, y)$ and $\sigma(x, b)$ calculated from Eqs. (4.16)-(4.24) are plotted in Fig. 4.2 for some a/b values. In this figure the pole density diverge near the corners as $\delta^{-1/3}$, where δ is the corner distance. Moreover, close to $x = 0$ the pole density depends linearly on x, being the linear region wider for higher a/b. These σ features, which were already used for other geometries, such as cylinders [61, 2, 3] and finite square bars [2], are very useful to optimize the finite elements calculations presented in §4.2.

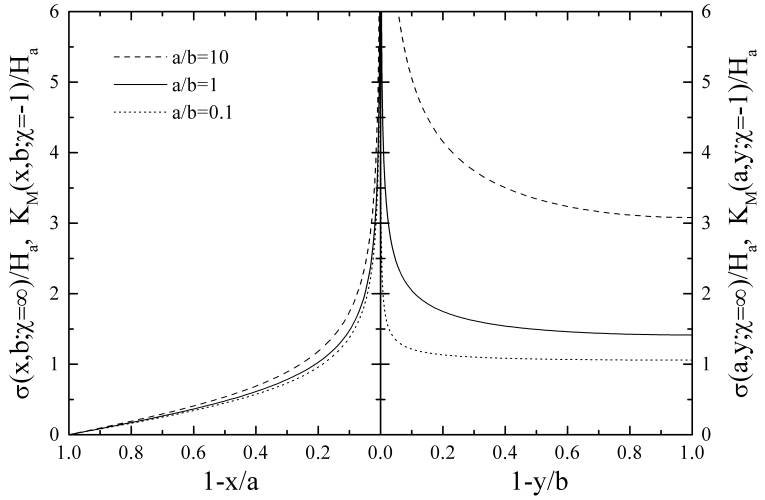

Figure 4.2: Surface pole density of the prism in Fig. 4.1(a) with infinite susceptibility $\sigma(x, y; \chi = \infty)$ and sheet current on the prism in Fig. 4.1(b) with -1 susceptibility $K_M(a, y; \chi = -1)$ for three different a/b values.

Volume average magnetization and demagnetizing factors

The average magnetization $M_{\rm mid,vol}$ can be directly calculated from the obtained surface pole density by means of Eqs. (3.8)-(3.10), changing z by x for the present geometry. After doing the corresponding integrations, we obtain [54, 65]

$$M_{\rm av}(z) = \frac{2H_{\rm a}\sin\theta}{b} \qquad (\arcsin k \le \theta \le \pi/2), \tag{4.25}$$

$$M_{\rm mid} = \frac{2H_{\rm a}}{b}, \tag{4.26}$$

$$M_{\rm vol} = \frac{\pi k'^2 H_{\rm a}}{ab}. \tag{4.27}$$

As explained in Sec. 2.2.2, for LHI materials the demagnetizing factors can be calculated directly from $M_{\mathrm{mid,vol}}$ by means of Eq. (2.39). Using the above $M_{\mathrm{mid,vol}}$ results and the a and b expressions in Eqs. (4.18) and (4.19), we obtain the demagnetizing factors formulae

$$N_{\mathrm{f}}(\chi=\infty) = E(k) - k'^2 K(k), \tag{4.28}$$

$$N_{\mathrm{m}}(\chi=\infty) = \frac{4}{\pi}\frac{[E(k)-k'^2K(k)][E(k')-k^2K(k')]}{k'^2}, \tag{4.29}$$

where $k'^2 = 1-k^2$ and the parameter k is related to a/b by means of Eq. (4.20).

4.1.3 Perfectly shielded infinitely long prism

This case, which correspond to $\chi=-1$ (§2.1.3), can be easily solved from the results for $\chi=\infty$ thanks to the conjugate relations, presented in Sec. 4.1.1.

Sheet current, volume average magnetization and demagnetizing factor

As explained in Sec. 4.1.1, the surface pole density in a prism with susceptibility χ^* and applied field in the x direction is related to the sheet current for another prism with susceptibility $-\chi^*/(1+\chi^*)$ and applied field in the y direction. Then, from σ for $\chi=\infty$ in Eqs. (4.16) and (4.17) and the relation in Eq. (4.8) we obtain the sheet current

$$K_M(a,y) = \frac{H_{\mathrm{a}}\cos\theta}{\sqrt{k^2-\sin^2\theta}} \qquad (0\le\theta\le\arcsin k), \tag{4.30}$$

$$K_M(x,b) = \frac{H_{\mathrm{a}}\cos\theta}{\sqrt{\sin^2\theta-k^2}} \qquad (\arcsin k\le\theta\le\pi/2), \tag{4.31}$$

where θ is related to x and y by means of Eqs. (4.22) and (4.21), respectively. The sheet current K_M for $\chi=-1$ is plotted in Fig. 4.2 for several a/b aspect ratios.

Since for $\chi=-1$ we know K_M but not σ, $M_{\mathrm{mid,vol}}$ cannot be calculated directly from σ by means of Eqs. (3.9) and (3.10), as done for $\chi=\infty$. However, M_{vol} can be deduced either from K_M and Eq. (4.11) or directly from the volume average magnetization for $\chi=\infty$ by means of the conjugate relation of Eq. (4.12), yielding to

$$M_{\mathrm{vol}} = -\frac{\pi k'^2 H_{\mathrm{a}}}{ab}. \tag{4.32}$$

Finally, we can apply the conjugate relation of Eq. (4.14) to derive N_{m} for $\chi=-1$ from the $\chi=\infty$ result. For the study of the susceptibility dependence of the demagnetizing factors, it is convenient to consider the same direction of the applied field for any χ. For $\chi=-1$ we only have to change a by b and b by a, which is the same as changing k by k' and k' by k. After doing these changes, we obtain from Eqs. (4.14) and (4.29) that

$$N_{\mathrm{m}}(\chi=-1) = 1 - \frac{4}{\pi}\frac{[E(k')-k^2K(k')][E(k)-k'^2K(k)]}{k^2}. \tag{4.33}$$

The fluxmetric demagnetizing factor N_f cannot be exactly calculated from K_M. This is so because neither M_mid nor $H_\mathrm{d,mid}$ can be calculated from K_M. The vector quantity that can be calculated from K_M is $\mathbf{B}_M$. However, the equation relating $B_{M,\mathrm{mid}}$ and N_f, Eq. (2.41), is not applicable for $\chi = -1$ because it yields mathematical indeterminations. Although N_f cannot be analytically solved exactly, it is possible to obtain an approximate formula for long samples in the applied field direction. As presented in [54, 65], such a formula is

$$N_\mathrm{f}(\chi = -1) \approx 1 - k', \tag{4.34}$$

which is valid for $a/b \geq 10$ if the applied field is in the x direction. Equation (4.34) can be deduced from taking into account that K_M is almost uniform on the surface parallel to $\mathbf{H}_\mathrm{a}$, except close to the corner.

4.1.4 Infinitely long rectangular prism with uniform magnetization ($\chi = 0$)

For completitude, we include the $N_\mathrm{f,m}$ formulae for an infinitely long strip with uniform magnetization, corresponding to the $\chi = 0$ case. This formulae can be calculated by direct integration of the demagnetizing field created by the uniform surface pole distribution $\sigma = \pm M$ on the sides perpendicular to the applied field [18]. Then, the demagnetizing factors $N_\mathrm{f,m}$ are

$$N_\mathrm{f}(\chi = 0) = \frac{2}{\pi} \arctan \frac{2b}{a} - \frac{a}{2\pi b} \ln\left(1 + \frac{4b^2}{a^2}\right), \tag{4.35}$$

$$N_\mathrm{m}(\chi = 0) = \frac{1}{2\pi}\left[4 \arctan \frac{b}{a} + \frac{2a}{b} \ln \frac{a}{b} + \right. \\ \left. + \left(\frac{b}{a} - \frac{a}{b}\right) \ln\left(1 + \frac{a^2}{b^2}\right)\right], \tag{4.36}$$

where a and b are the cross-section semisides parallel and perpendicular to the applied field, respectively.

4.2 Numerical calculations for arbitrary susceptibility

In this section we present the formalism to adapt the general method presented in Sec. 3.2 to infinitely long rectangular prisms with arbitrary χ. The most important issue of this adaptation is the surface division, which has been optimized to minimize the discretization error comparing to the analytical results. After doing this adaptation, we present the $N_\mathrm{f,m}$ numerical results for a wide range of χ and the a/b aspect ratio. The discretization error in the numerical calculations is estimated by comparing to exact analytical formulae and by using the conjugate relations in Sec. 4.1.1.

4.2.1 Formalism

Let us consider a rectangular prism (or strip) infinitely long in the z direction with arbitrary susceptibility χ and cross-section $2a \times 2b$ immersed into an applied field $\mathrm{H_a}$ in the x direction, Fig. 4.1.

In order to determine the surface pole density $\sigma(x, y)$ we use the numerical model described in Sec. 3.2. For the strip geometry we used the original numerical method, so that we did not consider the demagnetizing field average on the elements[3] (§3.2.1). To apply this model to the strip geometry, we divide its surface into n rectangular elements infinitely long in the z direction an with finite width in the x or y direction, depending on the side where the element belongs to, Fig. 4.1. Moreover, thanks to the system mirror symmetries, the pole density $\sigma(x, y)$ is antisymmetric in the x direction and symmetric in the y one. Then, the independent variables can be reduced to the surface pole density on the elements in the $x, y \geq 0$ region. If we consider this, we can keep the formalism for the linear equations set (3.5) by appropriately adapting the factors N_{n}^{ij}. The analytical expressions of the factors N_{n}^{ij} and the details of the numerical calculation method can be found in [13, 65].

In the following section we present the main issue to adapt the numerical method to infinitely long prisms, which is the surface division into elements with uniform σ.

4.2.2 Surface division into elements

The infinite prism is divided into $2n_x+1$ and $2n_y$ elements on the $y = \pm b$ and $x = \pm a$ surfaces, so that the total number of elements is $n = 2n_x + 2n_y + 1$. For the division in the x direction we set an element centered at $x = 0$ with zero pole density in order to avoid that an element border belong to the midplane. We proceed in this way since the demagnetizing field in the elements border diverge due to the surface pole density discontinuity, so that if the midplane contains an element border there is an important error in N_{f}. Moreover, the division is done by keeping the system mirror symmetries. Then, the total number of independent variables are $n' = n_x + n_y$.

For uniform magnetization, $\chi = 0$, σ is uniform in the sides $x = \pm a$ and zero in $y = \pm b$. However, for extreme values of susceptibility, $\chi = \infty, -1$, the surface pole density strongly depends on the position. In section 4.1.2 we presented the exact analytical expression for the surface pole density on a strip with $\chi = \infty$, which diverge as $\delta^{-1/3}$ and is linear with x close to $x = 0$ (Fig. 4.2). In a similar way, preliminary σ results for several χ show that σ diverge in the corner as a power law except for $|\chi| \ll 1$. Moreover, the cases for $\chi = \infty$ and $\chi = -1$ present the highest power law exponent in magnitude, so that the divergence near the corner is sharper. Since we assume that σ is uniform on the elements, a surface division with more elements near the corner reduces the discretization error.

[3] In our published calculations for strips [13, 65], we did not use $\mathbf{H}_{\mathrm{d}}$ averages on the elements even though the corresponding D_{n}^{ij} factors can be calculated analytically, because for this geometry, the results using the original model are already satisfactorily accurate.

If we already know $\sigma(x,y)$, as we do for $\chi = \infty$, we can have two types of cell divisions, namely, (i) uniform pole intensity, $\sigma^i \Delta x_i$ or $\sigma^j \Delta y_j$, and (ii) uniform pole-density increment, $\sigma_{i+1} - \sigma^i$ or $\sigma_{j+1} - \sigma^j$. The division used in [3] for cylinders is basically of type (i). In the present work, type (ii) is used, since compared with the exact $N_{\rm f,m}$ for $\chi = \infty$ and -1 calculated analytically, type (ii) results in smaller error in the final results.

For simplicity, we use artificial σ distributions,

$$\begin{aligned} \sigma(x) &= (1-x/a)^{-1/3} - (1+x/a)^{-1/3} + q_x x/a, \\ \sigma(y) &= (1-y/b)^{-1/3} - (1+y/b)^{-1/3} + q_y y/b, \end{aligned} \tag{4.37}$$

to calculate the cell divisions on the $y = b$ and $x = a$ surfaces, respectively. Since type (ii) involves a uniform division of $\sigma(x)$ or $\sigma(y)$ from the center to the corner, where $\sigma(x = a) = \sigma(y = b) = \infty$, we have to make a nonzero cutoff (δa or δb) close to the corner so that the cells can extend over the entire surface. To consider such a cutoff in the artificial σ functions and to make a division which cover the whole surface, we can modify Eqs. (4.37) as

$$\begin{aligned} \sigma'(x) &= \sigma\left(x\frac{a+\delta a}{a}\right) \\ \sigma'(y) &= \sigma\left(y\frac{b+\delta b}{b}\right). \end{aligned} \tag{4.38}$$

The determination of n_x and n_y is made under the conditions of $n_x + n_y = 400$ and $n_x/n_y \approx a/b$ with a minimum n_x or n_y equal to 40. For different values of χ and a/b, the values of q_x and q_y are chosen between 3 and 20 and $\delta a/a$ and $\delta b/b$ are chosen between 1/260 and 1/3000. They are determined iteratively by comparing the final results of $N_{\rm f,m}$ with the exact analytical formulae for $\chi = \infty, 0, -1$ of Eqs. (4.29), (4.28), (4.33), (4.35) and (4.36).

4.2.3 Demagnetizing factors results and discussion

The final results for $N_{\rm f,m}$ have been calculated for a χ and a/b values in such a way that the conjugate relations for $N_{\rm m}$ in Eq. (4.14) can be checked from the calculated $N_{\rm f,m}$ values. Then, we choose $\chi^* = 1.5, 9, 99, 999, 10^9 \sim \infty$ and $a/b = 1, 2, 5 \times 10^m$ for $0.001 \leq a/b \leq 1000$. In Refs. [13, 65] we reported tables containing all the calculated numerical results. To illustrate part of this data, we present in Figs. 4.3 and 4.4. In Fig. 4.3 we plot $N_{\rm f,m}$ and $1 - N_{\rm f,m}$ as a function of a/b, while in Fig. 4.3 we present the demagnetizing factors as a function of the susceptibility χ. The figure for $1 - N_{\rm f,m}$ is included since for some susceptibilities, such as $\chi = -1$, the factor $1 - N_{\rm f,m}$ is more relevant than $N_{\rm f,m}$.

General trends

From Figures 4.3 and 4.4, we can describe the general features of $N_{\rm f,m}$ as a function of a/b and χ, as it was done for cylinders [3]. Then, for infinite prisms we obtain the

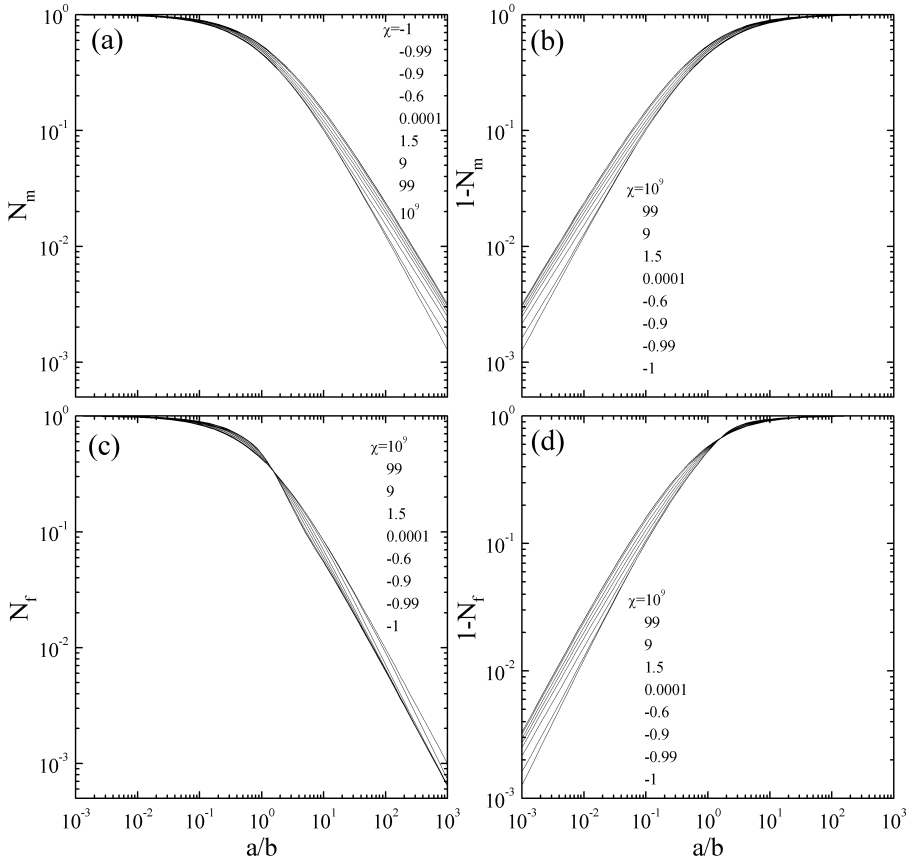

Figure 4.3: Demagnetizing factors numerical calculations for $N_{\rm m}$(a), $1-N_{\rm m}$(b), $N_{\rm f}$(c) and $1-N_{\rm f}$(d) for infinitely long rectangular prisms as a function of a/b for several χ.

following general $N_{\rm f,m}$ properties:

1. At any given χ, $N_{\rm f,m}$ decrease with increasing a/b. This is consistent with the known fact that the demagnetizing factors for an infinite sample with applied field in the infinite direction are zero.

2. $N_{\rm m} > N_{\rm f}$ at any given χ and a/b.

3. At any a/b, $N_{\rm m}$ decreases with increasing χ.

4. $N_{\rm f}$ decreases and increases with increasing χ at $a/b < 1.5$ and $a/b > 1.7$, respectively. This makes the following order of $N_{\rm f,m}$ change with χ:

$$\begin{aligned} N_{\rm m}(-1) \;&>\; N_{\rm m}(0) > N_{\rm m}(\infty) > N_{\rm f}(\infty) > \\ &\quad\; N_{\rm f}(0) > N_{\rm f}(-1) \qquad (a/b > 1.7), \\ N_{\rm f,m}(-1) \;&>\; N_{\rm f,m}(0) > N_{\rm f,m}(\infty) \qquad (a/b < 1.5). \end{aligned}$$

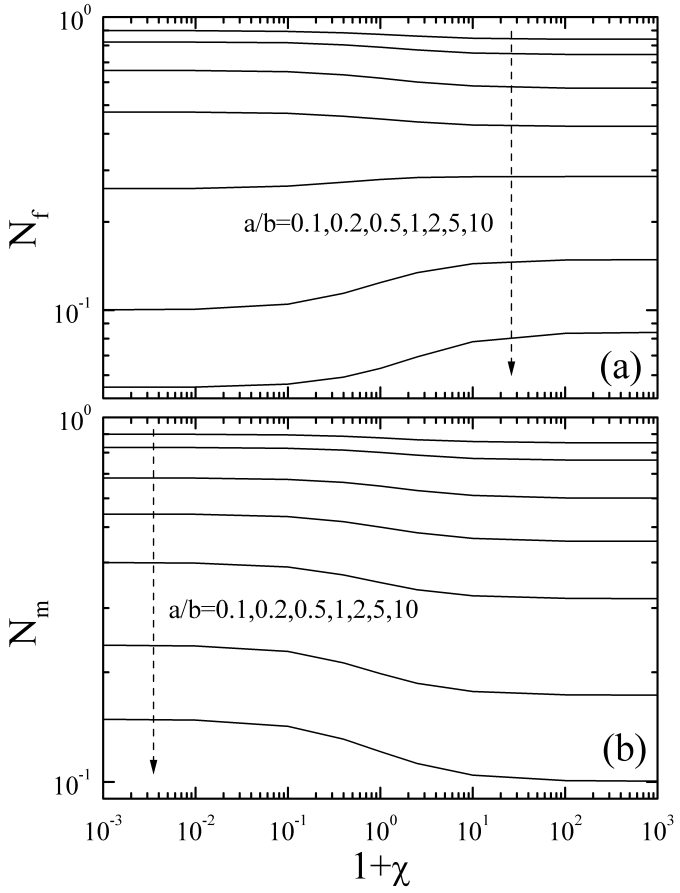

Figure 4.4: Numerical calculations for $N_{\rm f}$(a) and $N_{\rm m}$(b) for infinitely long rectangular prisms as a function of $1+\chi$ for several a/b values.

5. For $a/b > 0.7$, $N_{\rm m}/N_{\rm f}$ increases with increasing a/b and decreasing χ; for $a/b < 0.5$, $N_{\rm m}/N_{\rm f}$ decreases with decreasing a/b and decreasing χ.

6. For high a/b, $a/b > 10$, the minimum χ for $N_{\rm f}(\chi) > 0.99N_{\rm f}(\infty)$ and $N_{\rm m}(\chi) < 1.01N_{\rm m}(\infty)$, that is, the minimum susceptibility that can be taken as infinity concerning the demagnetizing factors, is $\chi \approx 10a/b$ and $\approx 6a/b$, respectively.

Error analysis

The discretization error of the $N_{\rm f,m}$ numerical calculations for $\chi = -1, 0$ and ∞ can be checked by comparing to the exact analytical results in Sec. 4.1. As explained in Sec. 3.3, the error of $N_{\rm f,m}$ must be more strictly defined as the maximum one between $N_{\rm f,m}$ or $1 - N_{\rm f,m}$.

After doing such a comparison, we find that the corrected value $N^c_{\rm f,m}$ calculated from $N^s_{\rm f,m}$ and $N^v_{\rm f,m}$ improves a lot comparing to the original results for almost all cases. The

improvement is vital for long samples ($a/b \geq 10$) with $\chi = \infty$, for which the best result between $N^s_{\mathrm{f,m}}$ and $N^v_{\mathrm{f,m}}$ can have up to a 15% error. The only cases which the correction $N^c_{\mathrm{f,m}}$ does not improve the calculations are for $\chi = -1$ and $a/b \leq 0.5$, for which the N^v_{m} result has higher accuracy. For this reason, the correction is used for any χ and a/b except for $\chi \leq -0.6$ and $a/b \leq 0.5$. The maximum error compared to exact analytical formulae are always for N_{m} (or $1 - N_{\mathrm{m}}$), being -0.13% for $\chi = -1$ and $a/b = 1000$ and -0.11% for $\chi = \infty$ and $a/b = 0.001$, while for $\chi = 0$ the maximum error is only -0.01%.

Since the surface pole density nonuniformity is higher for $\chi = \infty$ and $\chi = -1$, the intermediate χ results are expected to have a lower error. For these χ values, the error can be estimated by means of the conjugate relation for N_{m} of Eq. (4.14), since the deviation from 1 in the right-side part of this equation must be due to error. When doing this, we checked that the error for intermediate susceptibilities is lower than for the maximum error for the extreme values of χ presented above.

4.3 Chapter summary and conclusions

First, in this chapter we present some conjugate relations between different infinite prisms with applied field $\mathrm{H_a}$ in the x and y direction, respectively. We find that when the prism susceptibilities obey some conjugation condition, σ and N_{m} for one prism equal to K_M and $1 - N_{\mathrm{m}}$ for the other, respectively. A similar conjugate relations can be found for cylinders, allowing to calculate N_{m} in the radial direction from already calculated results for the axial one.

Furthermore, exact analytical formulae for $\sigma(\chi = \infty)$, are presented, from which formulae for $N_{\mathrm{f,m}}(\chi = \infty)$ can be calculated. The derived conjugate relations allow to obtain exact formulae for K_M and N_{m} for $\chi = -1$, as well as $N_{\mathrm{f}}(\chi = -1)$ for long prisms in the applied field direction. Moreover, we find that $\sigma(\chi = \infty)$ diverges as $\delta^{-1/3}$ near the corner, where δ is the distance to the corner, while σ depends linearly on the position near the prism midplane.

In order to obtain the demagnetizing factors for susceptibility values other than ∞, 0 and -1, we adapt the numerical method presented in Sec. 3.2 to infinitely long rectangular prisms. The adaptation to this geometry can be optimized thanks to the exact analytical results for $\sigma(\chi = \infty)$, $N_{\mathrm{f,m}}(\chi = \infty, 0)$ and $N_{\mathrm{m}}(\chi = -1)$. Specifically, they allow to check the discretization error for $\chi = -1, 0, \infty$, so that an optimum surface division can be found. The conjugate relations were also used to estimate the error for the numerically calculated $N_{\mathrm{f,m}}$ at the intermediate χ values, so that the maximum error is found to be 0.15%.

Finally, the optimization of these 2D calculations for infinitely long prisms is very useful for the development of the more general 3D method for finite rectangular prisms, which is presented in the next chapter.

CHAPTER 5

Rectangular prisms

In this chapter we adapt the numerical method for demagnetizing factors calculations in Sec. 3.2 to the finite rectangular prism geometry. As mentioned above, this adaptation relies on both the experience achieved with infinitely long rectangular prisms and the use of average demagnetizing fields on the elements, rather than the value at their center only.

For a given finite rectangular prism, the 3D calculations for $N_{\mathrm{f,m}}$ require much more computation time than the 2D ones for an infinite rectangular prism. Moreover, while $N_{\mathrm{f,m}}$ for infinite rectangular prisms only depend on two parameters, χ and an aspect ratio, for finite rectangular prisms we must also consider the dependence on a second aspect ratio. These two features are the reason for which a complete study of $N_{\mathrm{f,m}}$ for finite rectangular prisms requires many more calculations than for infinite rectangular prisms. Also, the discussion of the $N_{\mathrm{f,m}}$ calculated data for finite prisms is more complicated than for infinite ones since for the former we have to consider three parameters, while for the latter we only have to consider two. For these reasons, we study first the specific cases of square bars, where we fix one of the aspect ratio parameters, and then the completely shielded rectangular prisms, which corresponds to $\chi = -1$.

The geometry of rectangular bars is very important because it is often met in practice for material research (for example, the shape of a cube is popularly regarded as a highly symmetric one after a sphere).

The case of perfect shielding, corresponding to $\chi = -1$, is relevant since it is actually a representative of χ values less than 0. This is so because all diamagnetic materials with constant χ have $-1 \ll \chi < 0$, so that their $N_{\mathrm{f,m}}(\chi)$ are practically the same as $N_{\mathrm{f,m}}(\chi = 0)$, and a significantly negative constant χ occurs only for completely shielded superconductors or normal conductors, where $\chi = -1$ everywhere in the body. Moreover, these calculations are useful to determine the error committed by using the

infinitely long approximation for finite samples, not only for the cases of perfect shielding [54, 13, 64, 68, 69] but also for superconductors in the critical-state model (chapter 7) [32, 33, 70, 71]. This discussion can be also very useful for experimentalists working on ac susceptibility measurements of superconducting tapes [69].

As to the values of $N_{\mathrm{f,m}}$ for rectangular prisms with $\chi > 0$, they are being calculated by the time of writing this thesis and will be presented and discussed elsewhere.

5.1 Method adaptation to rectangular prisms

We consider a rectangular bar of dimensions $2a \times 2b \times 2c$ in the x, y and z directions, respectively, with constant internal susceptibility χ and immersed in a applied field $\mathbf{H}_{\mathrm{a}}$ in the z direction.

The surface pole density and the demagnetizing factors are calculated by means of the numerical method described in 3.2, which implies a surface division into elements. Then, the rectangular prism is divided into n rectangular elements. For the general rectangular prism geometry, we use the improved method which consider demagnetizing field averages on the elements to calculate σ, so that the linear equations set (3.6) is considered, yielding more accurate $N_{\mathrm{f,m}}$ results. As for infinitely long rectangular prisms, the system has several mirror symmetries, so that the number of the independent variables n' can be reduced to the number of elements in the $x, y, z \geq 0$ region. To consider this simplification, the factors D_{n}^{ij} in Eq. (3.6) must be correspondingly modified [52, 53]. The analytical formulae used to calculate D_{n}^{ij} can be found in [52, 53].

The quantities $H_{\mathrm{d,mid,vol}}$ are calculated by means of the corresponding analytically calculated element contributions $h_{z,mid,vol}^{i}$ (formulae can be found in [52]) and Eqs. (3.11) and (3.12).

We use the $N_{\mathrm{f,m}}$ correction of Eq. (3.13) for all cases except for $c/\sqrt{ab} \leq 0.5$ and $\chi \leq -0.6$. For these latter cases the result for $N_{\mathrm{f,m}}^{v}$ is more accurate, according to the infinitely long strip calculations, §4.2.3.

5.1.1 Surface division

The surface elements are taken to be rectangular shaped. Their size in the z direction Δz depends only on the z coordinate of the position of the element center z_i, Δx depends only on x_i, and Δy depends only on y_i. In this way, the surface division into elements can be done as the composition of three independent line elements divisions. We take the same nonlinear line division in the z direction as done for infinitely long rectangular prisms in the direction parallel to the applied field (Sec. 4.2.2 or Refs. [13, 65]). Consistently, the line divisions in the x and y directions are done as in Sec. 4.2.2 for the direction perpendicular to the field.

The numbers of divisions in the x, y, and z directions, $2n_x, 2n_y$, and $2n_z + 1$, respectively, are chosen by fixing the total number of independent variables[1] $n' =$

[1] As for infinitely long rectangular strips, we make the z direction divisons in such a way that all the

$n_x n_y + n_x n_z + n_y n_z$, taking $n_x = n_y$, and assuming $n_z/n_x \approx c/\sqrt{ab}$. We also consider the restrictions of $n_z \geq (\sqrt{n'/3})/5$, $n_x \geq (\sqrt{n'/3})/5$ for $\chi > -0.5$ and $n_x \geq (2\sqrt{n'/3})/5$ for $\chi \leq -0.5$.

5.1.2 Error estimation

In Sec. 4.2.3 (and [13, 65]), the error in the calculated $N_{\mathrm{f,m}}$ was checked by comparing the results with those calculated analytically for several χ values. However, for the case of square bars there are only exact analytical formulae for $N_{\mathrm{f,m}}$ at $\chi = 0$ [66, 59]. Since the error for extreme χ values, $\chi = \infty, -1$, is at least one order of magnitude greater than for $\chi = 0$ (§4.2.3)[13], these analytical formulae are not useful for estimating the error for arbitrary χ. Consequently, an alternative error estimation method has to be found.

The error involved in finite elements methods is mainly due to the division of a continuous body into discrete elements. The discretization error of the calculated σ^i decreases with increasing the number of elements n, so that the limit of $n \to \infty$ would yield to the exact σ^i, and consequently, the precise solution of $N_{\mathrm{f,m}}$. Then, if we plot $N_{\mathrm{f,m}}$ as a function of $1/n$, the exact $N_{\mathrm{f,m}}$ value would correspond to $1/n = 0$. Furthermore, if $1/n$ is low enough, the $N_{\mathrm{f,m}}$ dependence on $1/n$ can be estimated as linear.

The error is estimated as follows. For each pair of χ and c/a values, two $N_{\mathrm{f,m}}$ calculations are done using different numbers of elements, $n^{(1)}$ and $n^{(2)}$ with $n^{(1)} > n^{(2)}$. Then, we regard the "exact" $N_{\mathrm{f,m}}$ value as the linear extrapolation of $N_{\mathrm{f,m}}(1/n)$ at $1/n = 0$, obtained from $N_{\mathrm{f,m}}(1/n^{(1)})$ and $N_{\mathrm{f,m}}(1/n^{(2)})$. Finally, the relative error of $N_{\mathrm{f,m}}$ is estimated as $[N_{\mathrm{f,m}}(1/n^{(1)}) - N_{\mathrm{f,m}}(1/n = 0)]/N_{\mathrm{f,m}}(1/n = 0)$, taking $N_{\mathrm{f,m}}(1/n^{(1)})$ as the final $N_{\mathrm{f,m}}$ value. For the calculations presented in this paper we have used $n^{(1)}$ being around 8×4800 and $n^{(2)}$ around 8×4000, so that the number of independent variables are 4800 and 4000, respectively.

If the $1/n$ dependence of $N_{\mathrm{f,m}}$ were exactly linear, we should use the extrapolated $N_{\mathrm{f,m}}(1/n \to 0)$ as the final result. However, this is not the case, and we can only use this technique to estimate the error roughly.

As discussed in Sec. 3.3, it is convenient to define the relative error as the highest between $N_{\mathrm{f,m}}$ and $1 - N_{\mathrm{f,m}}$.

5.2 Square bars with arbitrary susceptibility

A complete study of the rectangular bar geometry with arbitrary susceptibility requires a large number of numerical calculation, since three independent parameters (χ and two prism dimensions ratios) must be taken into account. Then, we start with the square bar case, for which one of the dimensions ratios is fixed. For this case, we restrict the study when the applied field is perpendicular to the square direction.

elements surrounding the midplane are centered at $z = 0$.

5.2.1 Demagnetizing factors calculations

The demagnetizing factors $N_{\mathrm{f,m}}$ have been calculated for a set of χ values chosen "symmetrically" according to the conjugate relations in Sec. 4.1.1, being the susceptibility specific values $\chi = -1, -0.999, -0.99, -0.9, -0.6, 0.0001, 1.5, 9, 99, 999$ and 10^9. For each χ value, N_{f} and N_{m} are calculated for the c/a ratio $0.01 \leq c/a \leq 100$. The results are listed in Tables 5.1 and 5.2 for N_{f} and N_{m} [52], respectively. In order to show their features, curves of N_{f} and $1 - N_{\mathrm{f}}$ versus c/a are plotted in Figs. 5.1(a) and 5.1(c), and curves of N_{m} and $1 - N_{\mathrm{m}}$ versus c/a are plotted in Figs. 5.1(b) and 5.1(d).

Table 5.1: Fluxmetric demagnetizing factor, N_{f}, of a square bar with dimensions $(2a \times 2a \times 2c)$ magnetized along the c dimension. Results for N_{f} are multiplied to 10^5. For simplicity, $\chi = 0.0001$ and 10^9 are replaced by $\chi = 0$ and ∞, respectively.

c/a	$\chi=-1$	-0.999	-0.99	-0.9	-0.6	0	1.5	9	99	999	∞
0.01	97910.8	97899.1	97807.1	97361.9	96870.5	96481.5	96097.3	95694.0	95495.9	95472.6	95470.0
0.02	95985.3	95974.4	95883.7	95317.9	94526.6	93842.3	93148.4	92412.8	92050.3	92007.5	92002.6
0.05	90843.1	90833.6	90749.9	90082.6	88794	87499	86125	84649	83917	83830	83820
0.1	83651	83642	83561	82842	81185	79331	77297	75089	73989	73858	73843
0.2	72227	72217	72131	71346	69423	67170	64647	61883	60490	60323	60304
0.5	48891	48883	48807	48127	46533	44731	42731	40500	39336	39194	39178
1	26132	26132	26136	26159	26104	25873	25426	24725	24286	24229	24222
2	8434.7	8441.5	8501.6	9018.3	10091	11089	11959	12651	12900	12925	12928
5	1687.5	1688.6	1698.2	1786.7	2021.6	2363.2	2902.1	3805.0	4436.8	4521.8	4531.6
10	515.38	515.54	517.02	530.54	566.67	624.25	744.62	1124.4	1665.5	1767.4	1779.7
20	143.98	144.01	144.21	146.09	150.95	158.37	174.02	246.50	522.75	621.59	635.07
50	24.565	24.567	24.580	24.702	25.008	25.445	26.277	29.792	71.703	132.44	145.94
100	6.2606	6.2608	6.2625	6.2774	6.3142	6.3649	6.4566	6.7946	10.936	33.478	45.196

Table 5.2: Magnetometric demagnetizing factor, N_{m}, of a square bar with dimensions $(2a \times 2a \times 2c)$ magnetized along the c dimension. Results for N_{m} are multiplied to 10^5. For simplicity, $\chi = 0.0001$ and 10^9 are replaced by $\chi = 0$ and ∞, respectively.

c/a	$\chi=-1$	-0.999	-0.99	-0.9	-0.6	0	1.5	9	99	999	∞
0.01	97912.5	97900.9	97810.0	97378.5	96932.3	96603.9	96288.5	95954.4	95787.0	95767.1	95764.8
0.02	95994.1	95983.6	95895.5	95358.9	94656.4	94086.2	93518.2	92906.6	92598.0	92561.2	92557.0
0.05	90915.7	90907.0	90831.3	90240.5	89155	88100	86976	85730	85093	85017	85008
0.1	83973	83966	83900	83320	81999	80508	78819	76898	75905	75786	75772
0.2	73486	73479	73414	72813	71294	69419	67194	64612	63260	63097	63078
0.5	54629	54619	54530	53726	51808	49592	47089	44288	42835	42659	42639
1	38967	38954	38839	37835	35618	33333	31030	28713	27593	27460	27445
2	25091	25078	24962	23967	21862	19831	17937	16200	15427	15339	15329
5	12262	12254	12177	11515	10142	8831.4	7589.8	6376.6	5784.5	5713.4	5705.3
10	6653.1	6647.7	6600.1	6194.6	5363.3	4573.0	3802.8	2956.1	2417.8	2339.3	2330.1
20	3477.3	3474.3	3447.7	3222.0	2762.0	2326.2	1895.1	1383.7	955.90	869.45	858.47
50	1429.9	1428.6	1417.2	1320.8	1125.2	940.02	755.58	527.91	293.61	216.25	203.51
100	721.47	720.81	715.01	665.83	566.04	471.60	377.30	259.62	131.61	76.877	64.149

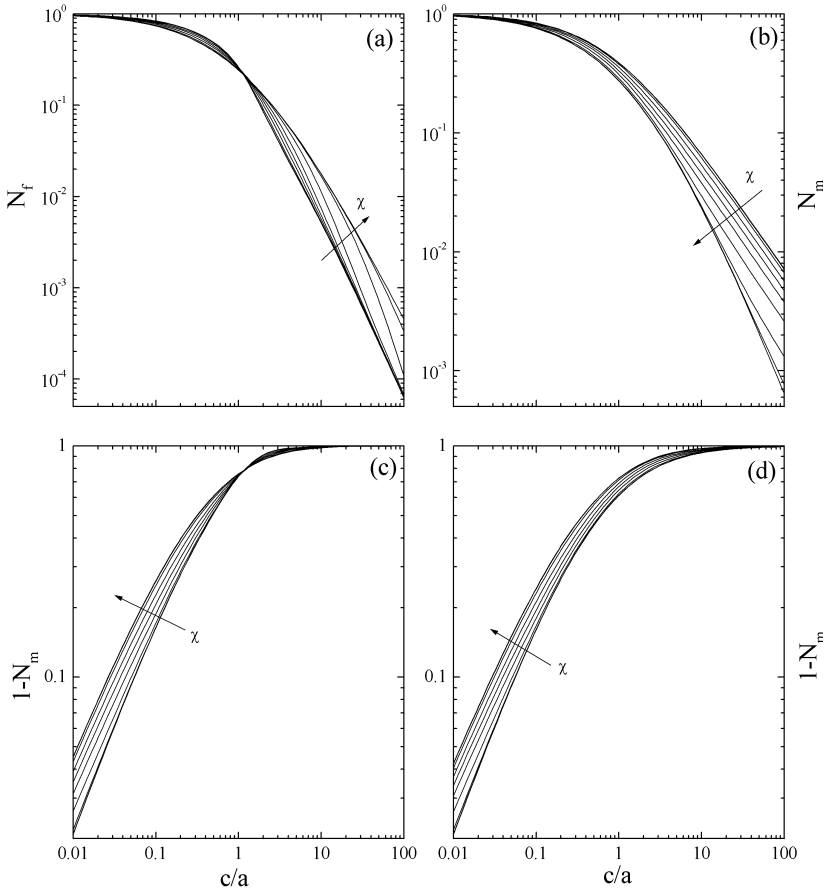

Figure 5.1: Demagnetizing factors for a square bar N_f (a), N_m(b), $1-N_\mathrm{f}$(c) and $1-N_\mathrm{m}$(d) as functions of c/a for $\chi = -1, -0.999, -0.99, -0.9, -0.6, 0, 1.5, 9, 99, 999$, and ∞. Each curve is a spline line passing through all the data points in Table 5.2 for a given value of χ. The arrow indicates the direction of increasing χ.

We found that the estimated discretization error in N_m is always greater than that for N_f. This is so because the contribution from σ in the vertices to $H_\mathrm{d,vol}$ is higher than to $H_\mathrm{d,mid}$ for proximity. Since the error in σ is greater near the vertexes, the error in $H_\mathrm{d,vol}$ is higher than to $H_\mathrm{d,mid}$ and so as to N_m and N_f. We next give some representative values for the error. For $\chi < 0$ the highest error in $N_\mathrm{f,m}$ is at $\chi = -1$ for the longest samples (high c/a), being 0.22%, while the maximum error in $1 - N_\mathrm{f,m}$ is -0.15% for the shorter samples and $\chi = -1$. For $\chi > 0$ the maximum error is for $\chi = \infty$ and $1 - N_\mathrm{f,m}$, being about 0.15% for lower c/a. We notice that in the aspect ratio range $0.2 \leq c/a \leq 5$ the error is lower than 0.05% in magnitude for any χ value. The estimated error for $\chi = 0$ is negligible for any c/a.

From Fig. 5.1 and the tabulated data we can see that the N_f and N_m general rules presented for infinitely long rectangular strips in Sec. 4.2.3 are essentially the same.

Rules 1, 2 and 3 are the same, while rule 4 and 5 are modified as follows. Concerning rule 4, now N_{f} decreases and increases with increasing χ at $c/a < 1$ and $c/a > 1.5$, respectively. Then, the order of $N_{\mathrm{f,m}}$ change with χ now is:

$$\begin{aligned} N_{\mathrm{m}}(-1) > N_{\mathrm{m}}(0) > N_{\mathrm{m}}(\infty) > \\ N_{\mathrm{f}}(\infty) > N_{\mathrm{f}}(0) > N_{\mathrm{f}}(-1) \quad (c/a > 1.5), \\ N_{\mathrm{f,m}}(-1) > N_{\mathrm{f,m}}(0) > N_{\mathrm{f,m}}(\infty) \qquad (c/a < 1). \end{aligned}$$

Rule 5 is modified, so that for $c/a \geq 0.5$, $N_{\mathrm{m}}/N_{\mathrm{f}}$ increases with increasing c/a and decreasing χ, while for $c/a \leq 0.2$, $N_{\mathrm{m}}/N_{\mathrm{f}}$ decreases with decreasing c/a and decreasing χ.

5.2.2 Comparison with existing results

There are only slight differences in the final digit between the numerically calculated $N_{\mathrm{f,m}}$ values for $\chi = 0$ given in Tables 5.1 and 5.2 and those given in [56] calculated from exact formulae.

Our numerical results may be compared with those for cylinders given in [3]. As discussed in [56, 2, 67], such a comparison is better to be made by defining the aspect ratio $\gamma = R/l$ for the cylinder and $\gamma = \sqrt{\pi}c/(2a)$ for the square bar, where R is the cylinder radius and $2l$ its length. When doing such a comparison we found [52] that for $\gamma > 1$ $N_{\mathrm{f,m}}$ for cylinders is slightly higher than for square bars, while $1 - N_{\mathrm{f,m}}$ for $\gamma < 1$ is significantly greater than cylinders, which can be up to 7% higher for the lowest γ. Moreover, such a comparison revealed that for $\gamma \leq 0.02$ some anomalies in $1 - N_{\mathrm{f,m}}$ existed for the cylinders calculations in [3]. These anomalies can appear since for those calculations only the relative error of $N_{\mathrm{f,m}}$ was considered but not that for $1 - N_{\mathrm{f,m}}$, see Sec. 3.3. An important conclusion we can extract from this i that for many purposes the results for square bars can be used for cylinders and vice versa [52].

5.2.3 Approximate conjugate relation for a cube

It is known that for any body with $\chi = 0$ the sum of the magnetometric demagnetizing factors along the x, y, and z directions is one, as discussed in Sec. 2.2.2 and [3]. In particular for a square bar with $c/a = 1$, and then, a cube, we have $3N_{\mathrm{m}}(\chi = 0) = 1$. From the data listed in Table 5.2, we find an interesting more general relation to be valid for a cube:

$$\frac{3}{2}\{N_{\mathrm{m}}(\chi = \chi^*) + N_{\mathrm{m}}[\chi = -\chi^*/(1 + \chi^*)]\} = 1 - \delta, \tag{5.1}$$

where $\delta \ll 1$, being $0, 0.0003, 0.0018, 0.0035$, and 0.0038 for $\chi^* = 0, 1.5, 9, 99$, and ≥ 999, respectively. These small nonzero values of δ cannot be due to the error in N_{m} calculation, since it is even smaller when $c/a = 1$, being 0 and ~ 0.0002 for $\chi = 0$ and $\chi \neq 0$, respectively. Since the two values of susceptibilities in Eq. (5.1) are conjugate as derived in Sec. 4.1.1 for the two-dimensional case, we refer to Eq. (5.1) with $\delta = 0$ as an approximate conjugate relation for the three-dimensional cube.

5.3 Completely shielded rectangular prisms

In the previous section we fixed one rectangular prism aspect ratio by considering square bars only. Now, the parameter that we fix is the susceptibility, $\chi = -1$, and we change the two prism aspect ratios. After presenting the $N_{\mathrm{f,m}}$ results, we will discuss them concerning actual measurements for superconducting tape prisms.

5.3.1 Demagnetizing factors calculations

The demagnetizing factors N_{m} and N_{f} have been numerically calculated at $0.01 \leq c/a \leq 100$ and $b/\max[c,a] = 1, 2, 5$, and 10. Together with the data for infinitely thin strips ($b \to \infty$) calculated previously in [54, 13] and presented in chapter 4, the results are listed in Table 5.3. In order to show their features, curves of N_{m} and $1 - N_{\mathrm{m}}$ versus c/a are plotted in Figs. 5.2(b) and 5.2(d), and curves of N_{f} and $1 - N_{\mathrm{f}}$ versus c/a are plotted in Figs. 5.2(a) and 5.2(b).

Table 5.3: Fluxmetric and magnetometric demagnetizing factors, N_{f} and N_{m}, of a rectangular prism with dimensions $2a \times 2b \times 2c$ and susceptibility $\chi = -1$ magnetized along the c dimension [53].

	N_{f}					N_{m}				
	$b/\max[c,a]$					$b/\max[c,a]$				
c/a	1	2	5	10	∞	1	2	5	10	∞
0.01	0.979125	0.983868	0.986330	0.987055	0.987752	0.979108	0.983859	0.986324	0.987050	0.987748
0.02	0.959941	0.968840	0.973525	0.974912	0.976223	0.959853	0.968793	0.973494	0.974884	0.976199
0.05	0.909157	0.928258	0.938673	0.941798	0.944730	0.908431	0.927862	0.938405	0.941563	0.944524
0.1	0.839734	0.871099	0.888972	0.894445	0.899584	0.836512	0.869275	0.887719	0.893340	0.898616
0.2	0.734864	0.781343	0.809595	0.818527	0.826967	0.722273	0.773830	0.804302	0.813823	0.822784
0.5	0.546293	0.609236	0.652644	0.667438	0.681738	0.488913	0.571093	0.624156	0.641688	0.658448
1	0.389667	0.454537	0.505128	0.523837	0.543053	0.261316	0.355763	0.424942	0.449520	0.474243
2	0.306389	0.346622	0.376887	0.388058	0.399699	0.143522	0.192848	0.230987	0.245067	0.259772
5	0.194122	0.212809	0.226717	0.231875	0.237263	0.056062	0.074173	0.088719	0.094203	0.100108
10	0.125881	0.135816	0.143260	0.146068	0.148540	0.031671	0.041182	0.048659	0.051463	0.054523
20	0.076982	0.082115	0.085975	0.087448	0.088655	0.017316	0.022250	0.026079	0.027510	0.029054
50	0.037788	0.039888	0.041463	0.042064	0.042566	0.007407	0.009434	0.010993	0.011575	0.012194
100	0.021384	0.022442	0.023234	0.023533	0.023798	0.003804	0.004828	0.005613	0.005906	0.006215

The error estimation for all cases is less than 0.2%. For the two-dimensional (2D) case with $b \to \infty$, the result for N_{m} is calculated by means of the exact formula of Eq. (4.33) and N_{f} corresponds to the numerical results presented in Sec. 4.2.3, having a maximum error of 0.1%.

In the above calculations for $2a \times 2b \times 2c$ prisms we used the aspect ratios c/a and $b/\max[c,a]$, although we could define the aspect ratios in several ways. This aspect ratio definition choice has been done to compare our results to the 2D models for infinitely long strips, such as those in Refs. [54, 13, 64, 68, 69, 32, 33, 70]. This is the reason why we use c/a as the primary aspect ratio for $\chi = -1$. The other aspect ratio is chosen as

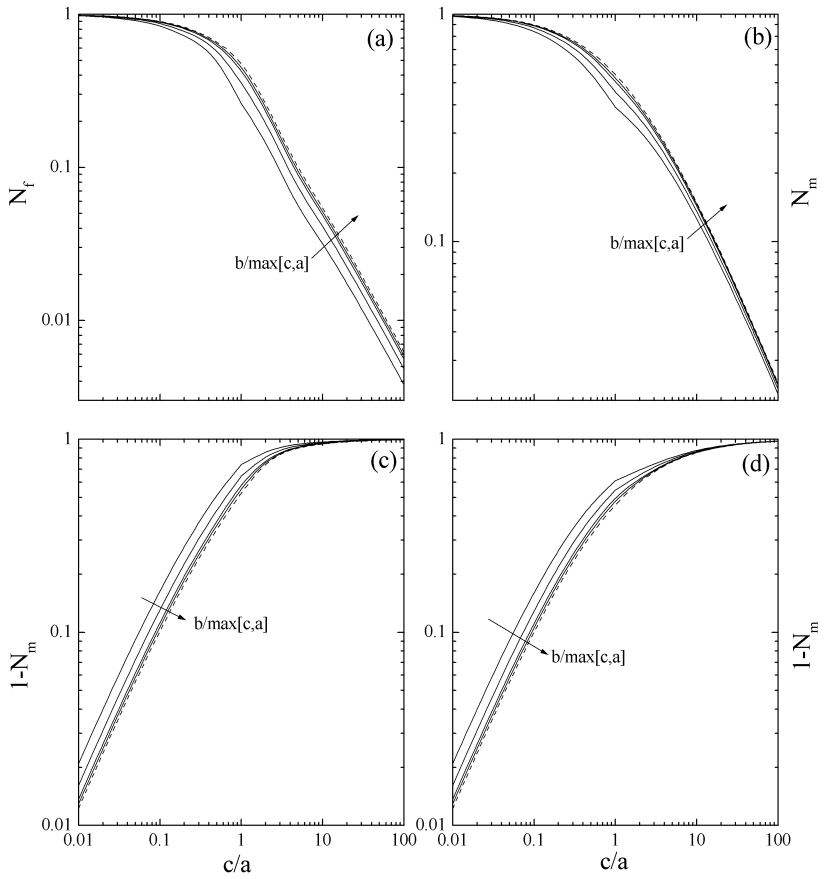

Figure 5.2: Demagnetizing factors for rectangular bars N_{f}(a), N_{m}(b), $1-N_{\mathrm{f}}$(c) and $1-N_{\mathrm{m}}$(d) as functions of c/a for $\chi=-1$ and $b/\max[c,a]=1,2,5,10$, (solid lines) and ∞ (dashed lines). Each solid line is made of two spline fits passing through the data points in Table 5.3 for a given value of $b/\max[c,a]$ in the regions of $c/a\leq 1$ and ≥ 1. The arrow indicates the direction of increasing $b/\max[c,a]$.

$b/\max[c,a]$ to study the effect of the finite length when comparing to 2D models. The use of this simple second aspect ratio is convenient from the experimental point of view, since larger dimensions can be measured more accurately. This aspect ratio definition is the cause of the kink appearing for $c/a=1$ in Fig. 5.2.

5.3.2 Application to superconductors research

The results are relevant to superconducting prisms in the Meissner state or the zero-field cooled critical state at low fields. Since highly conducting prisms may be completely shielded at sufficiently high frequencies, the results are also useful for them. Although both $N_{\mathrm{f,m}}$ are calculated for completeness, N_{m} is more useful in all these cases. An important quantity is the shape susceptibility $\chi_s^*=-1/(1-N_{\mathrm{m}})$ Sec. 3.3 [13], which is calculated for $0.01\leq c/a\leq 1$ as a function of b/c from the data in Table 5.3, as plotted

in Fig. 5.3.

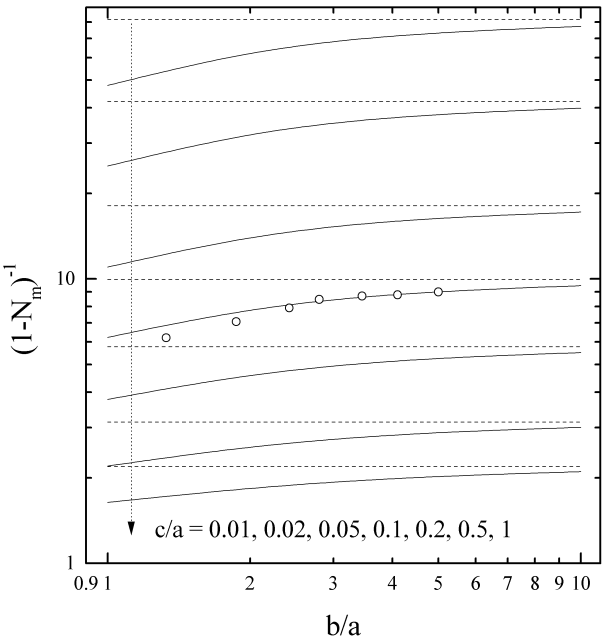

Figure 5.3: Shape susceptibility $-\chi_s^* = (1 - N_\mathrm{m})^{-1}$ for $\chi = -1$ as a function of b/a for $c/a = 0.01, 0.02, 0.05, 0.1, 0.2, 0.5$, and 1 (solid lines) compared with that for $b/a \to \infty$ (dashed lines). Open circles are for normalized experimental data in [69].

Fig. 5.3 can be very useful in experimental research of superconducting tapes. With the help of this figure, the 2D models assuming infinite strip length can be more strictly compared with experimental data. Roughly speaking, we see from Fig. 5.3 that if $c/a \leq 0.1$ as it is for most high-temperature superconducting tapes, $-\chi_s^*$ measured for samples with $b/a \approx 2$ and 5 will be lower than that of the corresponding infinitely long tape for about 20% and 10%, respectively. As an example, it is interesting to analyze the experimental results given in [69] for the sample length dependence of $-\chi_s^*$ of a mono-core Bi-2223/Ag tape as follows.

According to the description in [69], the elliptical cross-sectional dimensions of the core of the studied tape are similar to those of the core of rectangular cross-section tape, whose $2a = 1.4$ mm and $2c = 0.14$ mm. Therefore, we assume its $c/a = 0.1$, which corresponds to $-\chi_s^* = 10$ according to Fig. 5.3. Converting the sample length dependence given in Fig. 5.3 of [69] into b/a dependence assuming $2a = 1.4$ mm, and multiplying their $-\chi_s^*$ values by[2] 1.26, which may arise from the inevitable errors in dimensions and magnetic measurements, we obtain the renormalized experimental $-\chi_s^*$ as a function of b/a, as plotted in Fig. 5.3 by open circles. We see that the five high b/a circles agree well with the calculated $(1 - N_\mathrm{m})^{-1}$ versus b/a curve, from which we conclude that although after the fifth point, counted in the order of increasing b/a, the

[2]We choose this factor to fit the data to the corresponding $-\chi_s^*(b/a)$ curve.

result seem to saturate, as described by the authors of [69], it can still be less than that for $b/a \to \infty$ for 13%.

5.4 Chapter summary and conclusions

In this chapter we adapt the numerical method in Sec. 3.2 for $N_{\mathrm{f,m}}$ calculations to the 3D rectangular prism geometry. To achieve a good accuracy and to minimize the computation time, we use the improved method in Sec. 3.2 which uses average demagnetizing fields analytical formulae. The main method innovation which appears in this chapter is the error estimation, which is done by means of extrapolated $N_{\mathrm{f,m}}$ values to the infinite number of elements limit. This way of error estimation is necessary since no exact analytical results exist for $\chi \neq 0$.

Demagnetizing factors numerical results are obtained for square bars and perfectly shielded rectangular prisms ($\chi = -1$), having a maximum error of 0.22%.

After comparing the square bars results to the cylinders ones in [3] we find that in many cases $N_{\mathrm{f,m}}$ for square bars can be used for cylinders and vice versa. In addition, we find that the $N_{\mathrm{f,m}}$ results for a cube follow an approximate conjugate relation.

The results for rectangular prisms with $\chi = -1$ allows to obtain the sample length dependence of $N_{\mathrm{f,m}}$ for a fixed c/a aspect ratio. Moreover, the presented study of the shape susceptibility $-\chi_s^* = (1 - N_{\mathrm{m}})^{-1}$ is useful for both actual superconducting tapes experimental study and comparison to 2D models assuming infinite length. An agreement with experimental data has been found.

The calculations presented in this chapter and chapter 4 cover some of the lacks of demagnetizing factors results summarized in Sec. 3.4. The comparison between square bars and cylinders allows to find that the complete numerical results in [3] can be much improved at least for short samples, which is a case of practical importance for $\chi = -1$.